2017

PO2 DEPENDENCE OF OXYGEN CONSUMPTION IN SKELETAL MUSCLE OF DIABETIC AND NON-DIABETIC RATS

Alexander C. Liles
Virginia Commonwealth University

PO_2 DEPENDENCE OF OXYGEN CONSUMPTION IN SKELETAL MUSCLE OF DIABETIC AND NON-DIABETIC RATS

A thesis submitted in partial fulfillment of the requirements for the degree of Master of Science at the Medical College of Virginia Campus, Virginia Commonwealth University

By

Alexander C. Liles
B.S., Virginia Polytechnic Institute and State University, 2013

Director:
Roland N. Pittman, Ph.D.
Professor
Department of Physiology and Biophysics

Virginia Commonwealth University
Richmond, VA
May 2017

ACKNOWLEDGEMENTS

First, I would like to thank Dr. Roland N. Pittman for his guidance and support throughout this project. His willingness to drop everything at any time of the day to answer questions and offer advice made all the difference in my experience with this lab. His positive attitude is contagious and promotes a laboratory atmosphere that is both exciting and motivating. I always thoroughly enjoyed all of our conversations and hope to have many more in the future. I cannot thank him enough for all of his kindness and patience over this past year.

Secondly, I would like to thank Sami C. Dodhy for his constant willingness to teach and support me during my time with this laboratory. My project would not have been possible without the surgical expertise that he shared with me. When I had technical or conceptual questions, Sam was able to lead me to the answers in memorable ways that promoted a more thorough understanding. His sense of humor and friendship made my time in lab engaging and entertaining.

I would also like to thank Aleksander Golub for his vast scientific and technical knowledge. Without his support, I would not have been able to take measurements or properly analyze the data that were collected. I also thoroughly enjoyed listening to his stories about his past research and experiences in Russia.

I would like to thank Habiba Shah for being such a supportive friend throughout my project and keeping me motivated during long days and nights in the lab.

Finally, I am grateful to my family for their love, encouragement, and support this past year and always.

Table of Contents

List of Tables

List of Figures

Abstract

PO_2 DEPENDENCE OF OXYGEN CONSUMPTION IN SKELETAL MUSCLE OF DIABETIC AND NON-DIABETIC RATS

By: Alexander C. Liles

A thesis submitted in partial fulfillment of the requirements for the degree of Master of Science at the Medical College of Virginia Campus, Virginia Commonwealth University

Virginia Commonwealth University, 2017

Advisor: Roland N. Pittman, Ph.D.
Department of Physiology and Biophysics

Type 2 diabetes mellitus (T2DM) is a major medical problem around the world, affecting nearly 6% of the world's population. This study was an attempt to better understand physiological changes the disease may cause to the microcirculation and more specifically, to assess the PO_2 dependence of oxygen consumption in skeletal muscle of a diabetic animal model. The spinotrapezius muscles of Goto-Kakizaki (G-K) and Wistar control rats were used to measure interstitial PO_2 using phosphorescence quenching microscopy. The G-K rats spontaneously develop T2DM and serve as an appropriate model for the disease in humans. By rapidly arresting blood flow in the tissue and observing the resulting PO_2 changes, an oxygen disappearance curve (ODC) was created. The ODC was used to calculate oxygen consumption rate (VO_2) over the physiological range of PO_2 values. The resulting VO_2 vs PO_2 curves were analyzed using Hill's equation to fit the data and obtain values of several key parameters to

quantitatively describe the PO_2 dependence of oxygen consumption. When compared to healthy control rats, the G-K rats exhibited a significantly higher V_{max}, or maximum rate of oxygen consumption, compared to the Wistar rats. The two rat sub-strains had similar values for P_{50}, which indicates the PO_2 at half maximal consumption. The overall higher maximal rate of consumption by the diseased animals could be explained by some disconnect in the consumption of oxygen by the mitochondria and the normal corresponding production of ATP. In conclusion, it was demonstrated that *in situ* muscle tissue from both diabetic and non-diabetic rats had a PO_2 dependence of oxygen consumption over a wide range of PO_2 values and the muscles of diabetic animals consumed oxygen at a higher maximal rate.

Introduction

Cellular Need for Energy

The vast array of functions that are carried out by the cell in an organism require a constant input of energy in the form of adenosine triphosphate (ATP). In the presence of oxygen, oxidative phosphorylation within the mitochondria is the most efficient mechanism for production of this high-energy molecule. Since oxygen is required for this process to take place, the delivery of O_2 from the atmosphere to the cell is critical for maintenance of normal cellular function.

The Blood and Circulation

The requirement for a continuous and adequate supply of oxygen to the cell for energy production by the mitochondria is accomplished through an orchestrated effort between the cardiovascular and respiratory systems. Blood is oxygenated in the pulmonary capillaries of the lungs by the diffusion of oxygen from the nearby alveoli; the oxygenated blood is pumped by the heart through the circulation (Costanzo, 1998). Almost all of the oxygen in the blood is carried by the protein hemoglobin, contained within the red blood cells (RBCs), which has four binding sites for oxygen. When the oxygen bound to hemoglobin is delivered to tissue through the capillaries, the oxygen is released from the hemoglobin and can diffuse through the RBC cytoplasm, across the RBC membrane, through the plasma and across the capillary

wall into the interstitial fluid. Here the oxygen can move into cells and be used to generate ATP (Pishchany G, 2012).

The relationship between oxygen bound to hemoglobin (oxygen saturation, SO_2) and the partial pressure of oxygen (PO_2) can be described by the oxygen saturation (or dissociation) curve. The curve is sigmoidal in shape and illustrates the binding properties of hemoglobin. As PO_2 increases, the oxygen saturation also increases. In oxygen-rich arteriolar blood, on the one hand, hemoglobin is highly saturated with oxygen. On the other hand, oxygen is unloaded from the RBCs in areas with lower PO_2, such as capillary beds of skeletal muscle (Pittman, 2011). When certain physiological changes take place in the body (e.g., altered temperature, pH, PCO_2), the dissociation curve will shift to adjust the availability of oxygen to tissues. For example, an increase in temperature due to exercise shifts the curve to the right and therefore decreases the affinity of hemoglobin for oxygen. This allows oxygen to be released more easily from hemoglobin and increases its availability to muscle cells.

After oxygen is delivered to the microcirculation by oxygenated RBCs, it must make its way into the parenchymal cells by diffusion. The diffusion is driven by partial pressure gradients in oxygen that drive oxygen out of the capillaries, into the interstitial fluid, and eventually into the cell, as needed. As the mitochondria within the cell consume oxygen to make ATP, the PO_2 within the cell decreases and draws more O_2 into the cell from the interstitial fluid (Costanzo, 1998).

Glucose

Energy is required for normal functioning of body tissues, and glucose is the main substrate used by the body. Glucose is transported throughout the body in the blood and can be measured as "blood sugar." Serum glucose levels are normally tightly regulated through uptake and release mechanisms. Glucose can be stored in the liver as glycogen and then mobilized back to glucose as needed by the body. The β-cells of the pancreas release insulin when high blood sugar is detected in order to stimulate the uptake of glucose from the bloodstream. It has been shown that chronic exposure to high blood glucose can reduce the response of the β-cells, leading to complications like diabetes. Additionally, repeated stimulation by insulin and prolonged high levels of insulin can lead to insulin resistance, which is a major characteristic of Type 2 diabetes (White M.F., 1998).

As carbohydrates are consumed, they are broken down by the body and used to create energy. During glucose metabolism, glucose is oxidized to yield carbon dioxide and water while simultaneously producing energy in the form of ATP. The first step in the breakdown of glucose is glycolysis. As a result of glycolysis, pyruvate is produced. Under aerobic conditions, most pyruvate is oxidized and enters the Tri-carbolic acid (TCA) cycle, which has a high yield of ATP. For cellular respiration to be completed, NADH and $FADH_2$ produced during the earlier stages serve as electron donors in the electron transport chain (ETC). The ETC is an ordered series of proteins

embedded in the inner membrane of the mitochondria. Electrons are passed from one protein to the next in redox reactions that create a proton gradient across the membrane. This gradient is used to subsequently produce ATP. The ETC, along with this production of ATP via proton gradients, is known as oxidative phosphorylation. Oxygen is the terminal electron acceptor in the ETC and is therefore required for oxidative phosphorylation to occur. In anaerobic conditions, fermentation occurs, resulting in the production of lactate and a significantly lower ATP yield.

PO_2 Dependence of Oxygen Consumption

The mitochondria consume the vast majority (>95%) of oxygen that enters the cell for normal cellular respiration. The classic view of mitochondrial respiration is that consumption occurs at a constant rate regardless of shifts in the amount of oxygen in the area, unless the PO_2 falls below approximately 1 mmHg (Wilson, 1985). This view suggests that oxygen consumption is essentially independent of PO_2 under typical physiological conditions. Normal cellular respiration would be maintained even at relatively low or relatively high concentrations of oxygen as long as the PO_2 was above that critical level. This idea is supported by numerous *in vitro* studies that measured oxygen consumption rates in mitochondrial suspensions (Wilson, 1988). The oxygen dependence of respiration was later addressed using *in vivo* methods, which demonstrated that the mitochondria do not function in such an all-or-nothing or on/off manner (Golub, 2012). Based on these experiments, the rate of oxygen consumption appears to vary over a wide range of physiological PO_2 levels.

The PO_2 dependence of oxygen consumption can be illustrated by plotting oxygen consumption rate (VO_2) versus corresponding PO_2 values. In the context of using Michaelis-Menten kinetics to this PO_2 dependence, this allows the maximal rate of consumption (V_{max}) and also the half-maximal rate (at $PO_2 = K_m$) to be calculated. The classic view of PO_2 dependence suggests a K_m for oxygen consumption that is well below 1 mmHg (Wilson, 1988). However, recent *in vivo* studies concluded that the K_m in rat spinotrapezius muscle was approximately 10 mmHg (Golub & Pittman, 2012). This is a staggering difference that demonstrates oxygen consumption depends much more on varying PO_2 levels than previously thought.

Phosphorescence Quenching Microscopy

The *in vivo* studies described above involve measuring PO_2 of the interstitial fluid of skeletal muscle in rats using phosphorescence quenching microscopy (PQM) (Pittman R.N., 2012). PQM is an innovative approach to measuring oxygen tension that involves exciting a phosphor probe molecule from the ground state to an excited state using a brief flash from a light source, such as a laser. The excited phosphor molecule can return to the ground state by either emitting a photon (phosphorescence), or being quenched by oxygen (collisional quenching). The PO_2 can be calculated based on this relationship using the Stern-Volmer equation. The intensity of the phosphorescent light emission can be described by the following:

(1) $$I_{phos}(t) = I_{phos}(0)\, e^{-kt}$$

In this equation, $I_{phos}(t)$ is the intensity of the phosphorescent light emission, $I_{phos}(0)$ is the phosphorescence intensity at t = 0, and k is the phosphorescence (exponential) decay rate. Once the decay rate (k) is obtained, the PO_2 can be related to it with this formula:

(2) $$k = k_0 + k_q PO_2$$

The quenching coefficient (k_q) and the decay rate at zero PO_2 (k_0) are constants determined in separate calibration experiments (Golub, 2010).

When measuring the PO_2 of the interstitial space, the phosphorescent oxygen probe can be bound to albumin to prevent it from penetrating the cell and vasculature. When using a thin skeletal muscle, the dissolved probe can be loaded into the interstitium by simple topical application. After sufficient time has passed to allow for diffusion of the probe into the interstitial space (30-60 min), the tissue will be ready for determination of PO_2 by PQM (Nugent et al, 2015). Once PO_2 readings can be taken from the muscle, a "stop-flow" approach can be used to find the rate of oxygen consumption based on the subsequent decrease in oxygen tension over time. When

blood flow is halted, the tissue will continue to consume the available dissolved oxygen and the PO_2 will fall until it reaches approximately 0 mmHg.

Type 2 Diabetes Mellitus

Type 2 diabetes mellitus (T2DM) is characterized by a variety of dysfunctions that are caused by insulin resistance and inadequate insulin secretion. This results in chronic hyperglycemia and an assortment of related issues. It is a major disease that affects approximately 9.3% of the U.S. population and is increasing in prevalence worldwide (CDC). The major risk factors for T2DM include physical inactivity, poor diet, obesity, and increasing age. β-cells of pancreatic islets are involved in the secretion of insulin, which promotes the absorption of glucose from the bloodstream into the liver, fat, and skeletal muscle cells (Akash, 2013). The disease is known to occur as a consequence of β-cell dysfunction and reduction in β-cell size, which affects the secretion of insulin.

Goto-Kakizaki Rats: T2DM Animal Model

In order to study the effect of T2DM on the PO_2 dependence of oxygen consumption, a suitable animal model for the disease is required. Goto-Kakizaki (GK) rats are considered to be one of the best subspecies developed for the study of spontaneous T2DM (Akash, 2013). They were developed from selective inbreeding of Wistar rats, which serve as the best control group when research is being performed with these G-K rats.

GK rats share many significant characteristics with human diabetic patients including hyperglycemia, reduced β-cell mass, insulin resistance, and impaired glucose-induced insulin secretion (Akash, M, 2013). In order to help differentiate the impact of obesity and T2DM on hyperglycemia, they were developed as a non-obese model. G-K rat body weight is typically 10-30% lower than their age-matched Wistar control (Akash, M, 2013). Approximately 3 weeks after birth, these rats suddenly develop the characteristics mentioned above that accurately model T2DM. Similar to humans, the disease symptoms progress as they age. In adulthood, the rats often exhibit renal damage and proteinuria, which can be compared to diabetic nephropathy in humans. Overall, Goto-Kakizaki rats are a suitable non-obese animal model to investigate type 2 diabetes mellitus.

Purpose of Study

This project was initiated in order to study the PO_2 dependence of oxygen consumption in healthy and diabetic rats. It has been previously demonstrated in related *in vivo* studies that the oxygen consumption rate by the mitochondria of skeletal muscle cells is dependent on variations in PO_2 over a much wider physiological range than previously proposed (Golub AS, Pittman RN, 2012). To further investigate this concept, we decided to see if this dependence would change in a diseased animal model. Type 2 diabetes mellitus has broad metabolic effects primarily characterized by hyperglycemia and can be modeled well with Goto-Kakizaki rats. We sought to determine whether there was a difference in the oxygen dependence of respiration in the spinotrapezius muscles of healthy and diabetic rats by analyzing the disappearance rate of oxygen, following flow arrest, using phosphorescence quenching microscopy.

Materials and Methods

Animals and Surgical Preparations

Male Wistar rats (ENVIGO, Madison, WI, weight = 295.4 ± 23.2 g, N=5) served as the control group and male Goto-Kakizaki rats (Taconic Farms, Derwood, MD, weight = 249.8 ± 15.0 g, N=5) were used to characterize the PO_2 dependence of oxygen consumption in diabetic animals. Animals were housed in plastic cages with 2 rats per cage under a 12-hour/12-hour light/dark cycle. All animals received equal quantities of rat chow and water, which was provided by the Division of Animal Resources. There was continuous ventilation in a climate-controlled vivarium maintained at 20-23 degrees Celsius.

To perform the intravital microscopic studies, rats first underwent a surgical procedure to exteriorize the spinotrapezius muscle. Each rat was initially anesthetized with a Ketamine/Acepromazine (72/3 mg/kg) solution by intraperitoneal injection. After the rat was sufficiently anesthetized (about 10 minutes post-injection established by toe pinch), it was shaved in the bilateral inguinal creases, ventral neck region, and an area from the shoulder blades extending along the spine covering the spinotrapezius muscle using clippers. A depilatory cream (Nair, Church and Dwight Co., Inc., Ewing, NJ) was applied to remove any remaining hair. The animal was then placed under a stereomicroscope on a heating pad, to maintain core body temperature at 37 °C, in preparation for surgery. Blood glucose readings

were taken from the paw of the back left foot before and after each experiment using an AlphaTrak Blood Glucose Monitoring System (Zoetis Inc., Kalamazoo, MI). At the conclusion of the experiment, the rat was euthanized with Euthasol (150 mg/kg).

Femoral Vein Cannulation

Initially, an incision was made along the right inguinal crease and the right femoral vein was isolated. An incision was made perpendicular to the vein about half the diameter of the vessel. Before this incision was made, a knot was secured just distally to arrest blood flow through the vein. A cannula consisted of 26 cm of polyethylene tubing (PE 90) connected to a 6 ml syringe containing Alfaxan (Jurox Inc., Kansas City, MO, alfaxalone 10 mg/mL) and a 10 ml syringe containing heparinized phosphate-buffered saline (PBS). The Alfaxan was continually infused at 0.1 mg/kg/min for the duration of the experiment. This infusion rate was adjusted as necessary to maintain appropriate surgical depth of anesthesia based on toe pinch reflex and heart rate. The cannula was secured to the animal's leg using Transpore tape; and a cotton ball was taped over the incision to prevent drainage of any fluids. This cannula was also used to infuse Euthasol at the conclusion of the experiment to euthanize the animal.

Tracheostomy

Immediately following the femoral vein cannulation, the trachea was cannulated with polyethylene tubing (PE 240) to ensure a patent airway for the duration of the experiment. This incision was taped down and secured with a cotton ball. The animal breathed room air spontaneously.

S*pinotrapezius Muscle Preparation*

The spinotrapezius muscle was exteriorized following the procedures described by (Gray, 1973) and placed on a thermo-stabilized platform for intravital microscopy (Golub and Pittman, 2003). Initially, an incision was made longitudinally along the dorsal midline of the rat between the shoulder blades and extending down the spine to expose the underlying fascia. The fascia was removed carefully and a cauterizing pen was used to minimize bleeding. After the muscle was exposed, tissue hydration was maintained by topical application of PBS as needed. At this point, the muscle was carefully separated from the underlying fascia using curved scissors and placed on the platform. Surgical silk (size = 6-0) was sutured every 2 cm around the border of the muscle to aid with securing the muscle to the platform. Excessive stretching or manipulation of the muscle was avoided to prevent damage to any vessels.

Figure 1. Photograph of a spinotrapezius muscle prepared for intravital microscopy and PQM.

Phosphorescent Probe Application

Prior to mounting the heated animal platform to the microscope, 2 ml of the phosphorescent oxygen probe (Pd-meso-tetra-(4-carboxyphenyl)porphyrin (Oxygen Enterprises, Philadelphia, PA) conjugated to human serum albumin in PBS) was topically applied to the spinotrapezius muscle at a concentration of 10 mg/ml and allowed to diffuse into the muscle for 60 minutes. It can be assumed that the probe does not enter the muscle fibers because it was bound to albumin, which is too large to pass through the cell membrane. Any residual probe that entered the microvasculature would be immediately "washed out" by blood flow. Therefore, it was determined that measurements taken from exciting the probe that diffused into the tissue in this manner would be confined to the interstitial fluid space. After the probe was applied, the muscle was covered with a gas-impermeable film (Krehalon, CB-100; Krehalon Limited, Japan) to isolate it from the room air.

Phosphorescence Quenching Microscopy

After the probe was distributed within the interstitial space, the animal platform was mounted on an Axioplan-2 microscope (Zeiss, Germany) in preparation for phosphorescence quenching microscopy studies. To excite the probe, pulses from a laser were produced at a rate of 1 Hz. A photomultiplier tube collected the phosphorescence emitted from the excited probe and a colored-glass long-pass filter (OG 550, Edmund Optics) was in place to avoid extraneous excitation. A video camera

was also used to aid in visually selecting well-perfused sites in the muscle and ensure that the pneumatic tissue compression fully evacuated the RBC's from the site. The phosphorescence signal collected by the PMT was transmitted through an amplifier to an analog-to-digital converter. This allowed the phosphorescence decay curves to be analyzed by custom data processing software using the National Instruments platform. A PO_2 value was produced for each phosphorescence decay curve using the analysis software.

An additional consideration when measuring PO_2 using this technique is the photoconsumption of oxygen. As described in the introduction, singlet oxygen is produced by the interaction of the probe and O_2. The singlet oxygen can react with organic molecules and is therefore "consumed" by the method. This proportional reduction in PO_2 needs to be accounted for by calculating a coefficient (K) that is related to photoconsumption. This is accomplished by measuring PO_2 at two different excitation frequencies using a 5 s x 15 s high/low pressure cycling method (Nugent et al, 2015). For a total of 100 seconds, a series of 5 second compressions each followed by 15 seconds with no compression, alternating between the high and low frequencies were measured. The PO_2 changes were then compared to calculate the photoconsumption coefficient using the following formula:

(3) $$K = [(dP_n/dn)_1 - (dP_n/dn)_2]/[(FP_0)_2 - (FP_0)_1]$$

In Equation 3: *F* is the flash rate for each measurement, dP_n/dn is the rate of oxygen disappearance per flash at the given high or low frequency, P_0 is the steady state PO_2 at the given flash rate prior to pneumatic compression.

Phosphorescence Decay Curve Analysis

A non-linear fitting program was used for each phosphorescence decay curve that was based on the rectangular $P_{ISF}O_2$ distribution model (Golub et al., 1997). The fitting program was used to obtain a continuous line fit for each decay curve calculate the phosphorescence decay rate. The fitting equation used was as follows:

(4) $$I(t) = I_0 \exp\left[-\left(K_0 + K_q M\right)t\right] \sinh\left(K_q \delta t\right)/K_q \delta t + B$$

in which t is time in μs from the beginning of the decay, I(t) is the phosphorescence decay curve in volts, I_0 is the magnitude of the phosphorescence signal at t = 0, M is the average PO_2 (mmHg) in the region being measured, δ (mmHg) is the half-width of the uniform PO_2 distribution, and B (volts), is the baseline offset of the amplifier. K_0 and K_q serve as constants and have been determined from calibration experiments (Golub and Pittman, 2016) to be K_0 = 1.53 x 10^{-4} μs^{-1} and K_q = 4.3 x 10^{-4} μs^{-1} $mmHg^{-1}$.

Tissue Compression

An airbag mounted on the objective lens of the microscope was used to arrest blood flow in the spinotrapezius muscle. The airbag was rapidly inflated (<1s) to approximately 150 mmHg, which is higher than systolic pressure, causing blood flow to cease and extrude most of the red blood cells from that region. This was confirmed by visually inspecting the site using the video camera. After the tissue was compressed, a fall in PO_2 was observed as the tissue consumed the remaining dissolved oxygen. For each animal, five well-perfused sites were chosen to measure PO_2 during the compression cycle. Measurement sites were chosen based on specific criteria: it was required that the site was well perfused with continuous RBC flow and was not close to any large vessels.

To obtain a baseline PO_2 for each site, the PO_2 was measured for 10 seconds prior to compression. After the airbag was inflated, PO_2 continued to be measured for an additional 60 seconds in order to observe the complete disappearance of oxygen. The tissue was allowed to rest with no compression or excitation for 5 minutes between measurements at each site.

Analysis of Oxygen Consumption

For each site, an oxygen disappearance curve (ODC) was observed as the PO_2 decreased during compression. The rate of PO_2 change after the blood flow had been

arrested with the airbag was related to several factors. First, the tissue consumed O_2 as a part of normal respiration. Additionally, consumption by the method itself (photoconsumption) and O_2 diffusion into the excitation region had to be accounted for. It was important to account for these factors in order to accurately calculate the O_2 consumed specifically by tissue respiration.

The ODC was used to calculate the oxygen consumption rate (V_n) at a given PO_2, which is necessary to determine the PO_2 dependence of oxygen consumption. The relationship between V_n and PO_2 is described by the following formula:

(5) $$\frac{dP_n}{dn} = -V_n - KP_n + Z(P_n - P_n)$$

in which $\frac{dP_n}{dn}$ is the rate of O_2 disappearance per flash, K is the coefficient related to consumption by the PQM method, and Z is the coefficient related to inward diffusion of O_2 into the excitation region. The area being compressed is large enough so that the passive inward diffusion of O_2 can be neglected.

Statistics

The values expressed in tables and the text are mean ± SE (N). A t-test was conducted in comparisons between G-K and Wistar results to test for significance. Statistical significance was assigned for $p<0.05$.

Results

The goal of this study was to determine whether there was any difference in the oxygen dependence of oxygen consumption between diabetic and non-diabetic animals. These data were collected using the "flow arrest" approach described in the preceding Materials and Methods section.

Oxygen Disappearance Curves

Following each spinotrapezius muscle compression, an oxygen disappearance curve (ODC) was produced using the collected PO_2 data and flash number (proportional to time). These ODC's were corrected for consumption by the PQM method using Equation 3. During the first 10 seconds of collection, the muscle was not compressed and the baseline PO_2 was established. After 10 seconds, the airbag was inflated and the disappearance curve was created based on the decrease in PO_2.

Oxygen Disappearance Curve – Wistar Rat

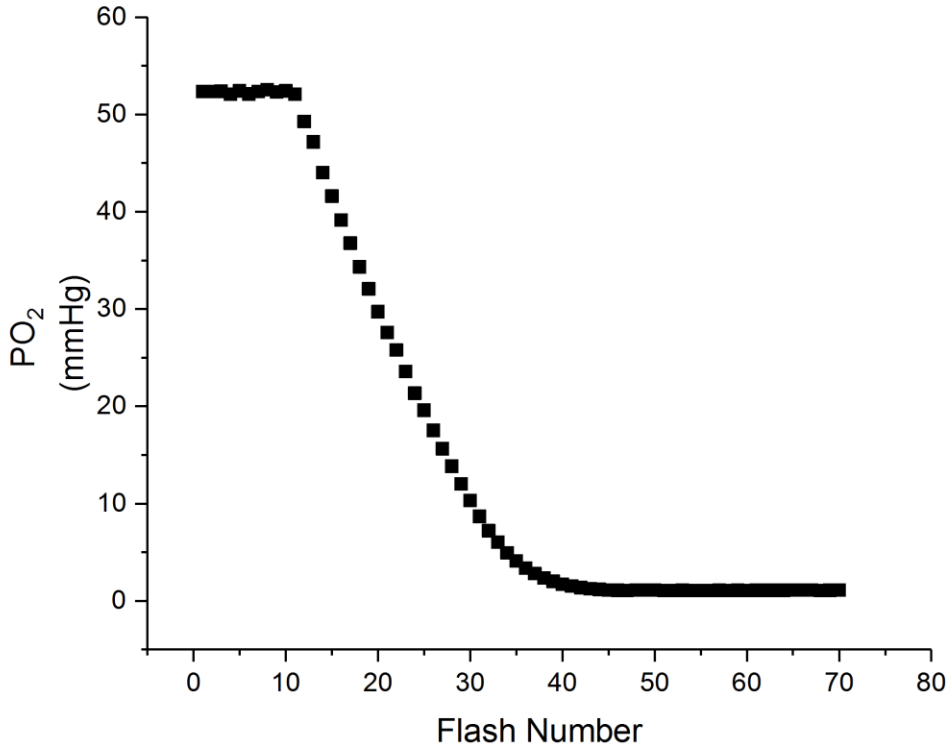

Figure 2. This is an example of a typical oxygen disappearance curve collected from a Wistar rat using the PQM method. The laser was flashed at 1 Hz, so a new PO_2 value was measured every second.

Oxygen Disappearance Curve - Goto-Kakizaki Rat

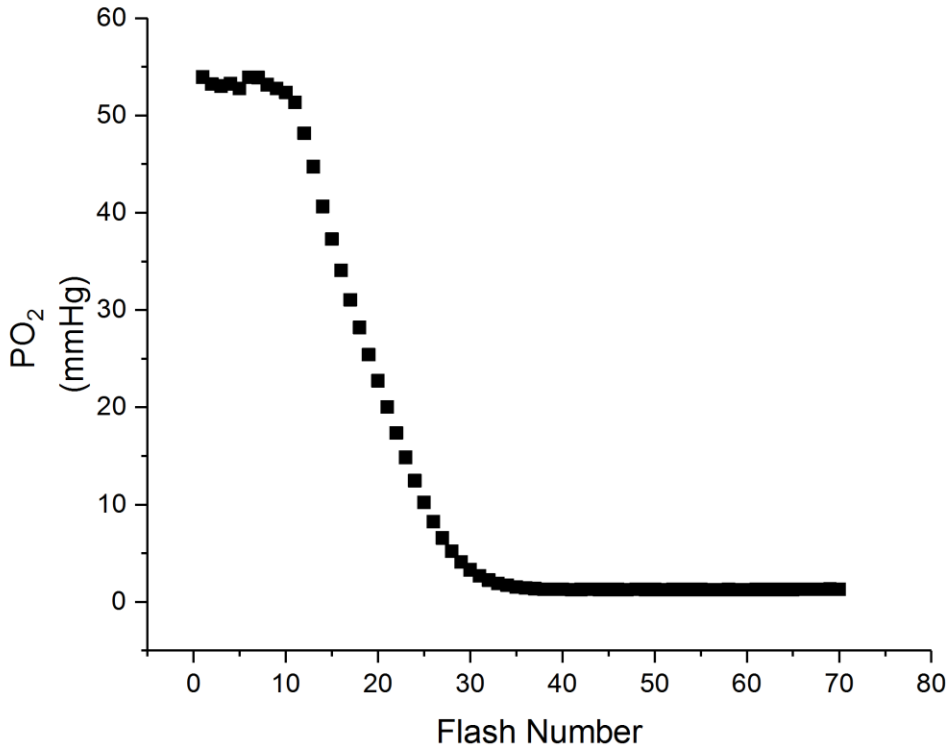

Figure 3: The oxygen disappearance curve above is a representative curve from a single site on the spinotrapezius muscle of a Goto-Kakizaki rat.

PO_2 Dependence of VO_2

The oxygen disappearance curves were used to calculate VO_2 for each PO_2 value. Plots of VO_2 vs. PO_2 were created and these plots were then fit with Hill's equation (Equation 6).

(6) $$\boldsymbol{VO_2 = \frac{Vmax \times P_n^a}{P_{50}^a + P_n^a}}$$

In Hill's equation, P_n represents the PO_2 at a given flash number in the ODC and VO_2, V_{max} is the maximal rate of respiration, P_{50} is the PO_2 at half-maximal respiration, and *a* is the Hill coefficient.

After fitting the data for the VO_2 vs. PO_2 plots with Hill's equation, the best-fit parameters, V_{max}, P_{50} and a, were obtained. The mean V_{max} for the Wistar control rats was 131.9 ± 8.7 (SE) nl $O_2/(cm^3$*s). The mean P_{50} in the control group was 8.0 ± 0.6 (SE) mmHg. The spontaneously diabetic Goto-Kakizaki rats had an average V_{max} of 215.9 nl $O_2/(cm^3$*s) with a standard error of 23.0 and the mean P_{50} was 8.5 mmHg with a standard error of 0.5.

VO_2 vs. PO_2 Plot – Wistar Rat

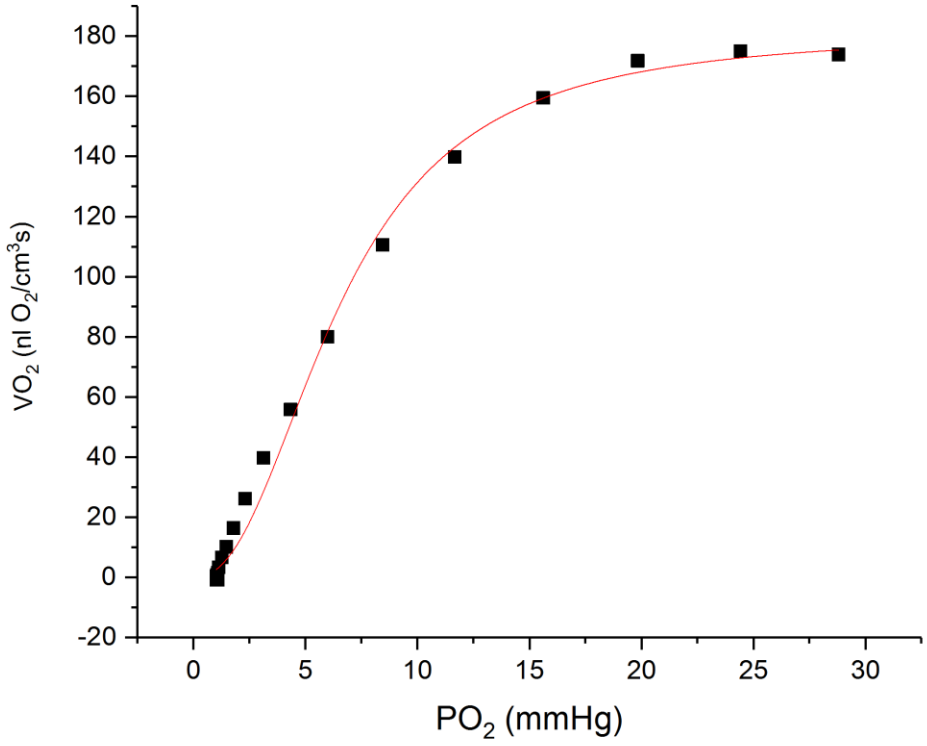

Figure 4. This is a typical plot of VO_2 vs. PO_2 that is used to assess the oxygen dependence of respiration in rat spinotrapezius muscle. The above example is taken from a single site on the spinotrapezius muscle of a Wistar rat. The Hill parameters calculated by fitting these data were as follows: V_{max} = 181.4 nl $O_2/(cm^3s)$, P_{50} = 6.5 mmHg, a = 2.3, r^2 = 0.99.

See *Appendix* for full collection of VO_2 vs. PO_2 plots from Wistar rats.

VO_2 vs. PO_2 Plot – Goto-Kakizaki Rat

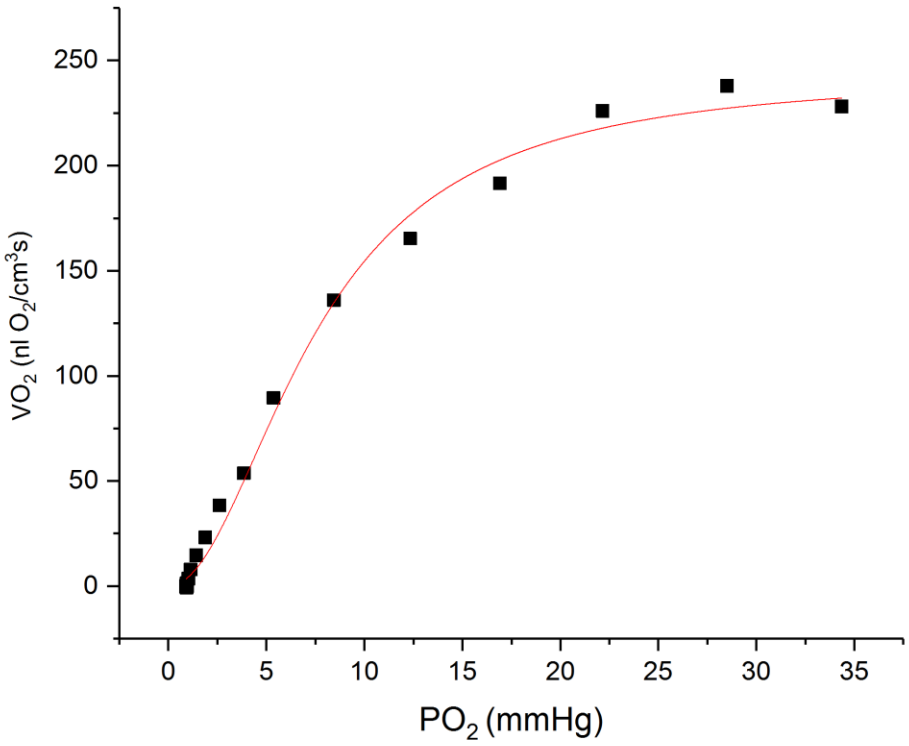

Figure 5. The above plot was derived from analyzing an oxygen disappearance curve measured from a Goto-Kakizaki rat. The Hill parameters calculated by fitting these data were as follows: V_{max} = 243.5 nl O_2/(cm^3s), P_{50} = 7.6 mmHg, *a* = 1.9, r^2 = 0.99.

See *Appendix* for a full collection of VO_2 vs. PO_2 plots from Goto-Kakizaki rats.

	Vmax (nl $O_2/(cm^3$*s))	**P50 (mmHg)**	**a**
Wistar (23)	131.9 ± 8.7	8.0 ± 0.6	2.1 ± 0.1
G-K (14)	215.9 ± 23.0	8.5 ± 0.5	2.1 ± 0.1

Table 1: The table above shows the best-fit values for V_{max}, P_{50}, and a (mean ± SE) for Wistar and Goto-Kakizaki rats. The maximal rate of oxygen consumption in the G-K rats was significantly higher than that of the Wistar controls.

(n) refers to number of curves

Blood Glucose

The blood glucose level of each rat was measured using an AlphaTrak Blood Glucose Monitoring System (Zoetis Inc., Kalamazoo, MI) before and after each experiment. The readings can be considered non-fasting because the rats had continuous access to food in their cages and their eating habits were not carefully monitored. The blood glucose level for the Wistar control group was 223.3 ± 29.9 (SE) mg/dL. The Goto-Kakizaki rats had a blood glucose level of 580.5 ± 42.0 (SE) mg/dL.

Rat Sub-strain	Wistar	Goto-Kakizaki
Glucose Level (mg/dL)	223.3 ± 29.9	580.5 ± 42.0

Table 2. Mean non-fasting glucose levels in Wistar and Goto-Kakizaki rats.

Discussion

Major Findings

The major finding in this project was that the maximal rate of oxygen consumption in rat spinotrapezius muscle measured using phosphorescence quenching microscopy was significantly higher in Goto-Kakizaki rats compared to Wistar controls: Goto-Kakizaki, V_{max} = 215.9 ± 23.0 nl $O_2/(cm^3$*s) and Wistar, V_{max} = 131.9 ± 8.7 nl $O_2/(cm^3$*s)). This finding indicates that, in an animal model for type 2 diabetes mellitus, a resting striated muscle has an elevated rate of oxygen consumption in the upper range of PO_2. The PO_2 at half maximal rate of consumption was not significantly different in Goto-Kakizaki and Wistar rats (Goto-Kakizaki, P_{50} = 8.5 ± 1.9 mmHg and Wistar, P_{50} = 8.0 ± 3.0 mmHg). Additionally, based on these results for P_{50}, it is important to note that the PO_2 dependence of oxygen consumption in rat spinotrapezius muscle does cover a wide range of physiological PO_2 values in both Wistar and the diseased animal model. Previous studies on the sensing of oxygen by isolated cells and mitochondria (Wilson, 1985) have shown that mitochondria consume oxygen at a constant rate regardless of oxygen tension until PO_2 falls below about 1 mmHg. The P_{50} values calculated in this study and previous studies on the spinotrapezius muscle of male Sprague-Dawley rats (Golub, A. S., & Pittman, R. N., 2003) suggest that the range of sensitivity to PO_2 is much wider. Furthermore, the range is consistently wide in the spinotrapezius muscles of spontaneously T2DM rats and Wistar controls.

Oxygen Disappearance Curves

The oxygen disappearance curves (examples in Figures 2 and 3) collected from both the Wistar and G-K rats clearly display the previously observed behavior of the spinotrapezius muscle from Sprague-Dawley rats in terms of oxygen consumption over time. The 10 seconds of data collected before airbag inflation/tissue compression show the baseline PO_2. This PO_2 value represents the amount of oxygen that is maintained in equilibrium in the interstitial fluid by the inflow of oxygenated blood through the microcirculation and consumption by the tissue. On average, the G-K rats had a higher baseline PO_2 compared to the Wistar controls. At 10 seconds, when the airbag was inflated and blood flow was arrested, that equilibrium was disturbed. There was no longer oxygen bound to hemoglobin flowing into the area, so the PO_2 immediately began to decrease in proportion to the rate of oxygen consumption by the muscle. The initial slope of the line is near linear, indicating that the rate of consumption is not very dependent on PO_2 at those levels. As the oxygen tension continues to drop, due to continued consumption without replenishment of oxygen from the blood, the line begins to curve downward exponentially until it reaches approximately zero mmHg. The point at which the line stops behaving linearly marks a critical point at which the tissue consumption rate starts to decrease with decreasing PO_2 levels. The difference in the time at initial compression to the time the curve reaches approximately 0 mmHg represents the total amount of time

required for the tissue to consume all the available oxygen in the interstitial space. This ranged from 30-45 seconds in both Wistar and G-K rats.

VO_2 vs. PO_2 Plots

Figures 4 and 5 display the plots of the PO_2 dependence of oxygen consumption for a Wistar and - rat, respectively. The data were fit with Hill's equation to provide a non-linear fit line and several key parameters. V_{max} is used to describe the maximum rate of consumption by the given muscle in the tissue region being measured. Another useful parameter for describing this relationship is P_{50}, which is equal to the PO_2 at half - maximal consumption rate. A higher P_{50} indicates that the oxygen consumption rate is dependent on a wider range of PO_2 values. On average, the G-K rats had a higher, but non-significant, P_{50}, compared to the Wistar rats.

Explanation for Increased V_{max} in G-K rats

If the skeletal muscle of diabetic rats consumes oxygen at a higher average maximal rate, one explanation could be that there is an "uncoupling" of O_2 consumption and ATP production in the mitochondria that leads to less efficient production of ATP and a higher requirement for oxygen. In that case, a given cell would need to consume more oxygen in order to produce the same amount of ATP required for normal cellular processes. This may lead to a higher maximal rate of

oxygen consumption in skeletal muscle at resting conditions. The term "mitochondrial uncoupling" can be used to describe any situation in which the electron transport chain is not used to produce ATP or create proton gradients (Mookerjee SA, 2010). If a situation were to arise in which oxygen was still being consumed through oxidative phosphorylation, but the proton gradient was not being created as efficiently and ATP was not being produced at the same rate, the cell may have to compensate by increasing the rate of respiration. This would make up for the decreased energy production and also consume oxygen at a higher rate, leading to a higher V_{max}.

In related studies, it has been shown that the mitochondria in diabetic rats are smaller and fewer in number (Morino K, 2005). This would logically suggest that overall consumption of oxygen by mitochondria in a particular cell or tissue would be lower than that of a healthy control. In fact, it has been demonstrated that muscle oxidative phosphorylation in diabetic rats was impaired (Kelley DE, 2002, Sivitz, William I, 2016). This appears contradictory to the results of this study, because decreased oxidative phosphorylation should result in less oxygen being consumed by the cell and less ATP being produced.

As described before, the classic view of ATP production involves oxidative phosphorylation and anaerobic glycolysis as separate processes that are carried out independently based on oxygen availability. In physiologically oxygen-rich environments, the cell will choose to produce energy more efficiently through oxidative phosphorylation and conversely, using glycolysis with the production of

lactate in environments where oxygen is unavailable. This either/or scenario fits well with the classic view that mitochondria consume oxygen at a steady rate throughout most of the physiological range until PO_2 drops below about 1 mmHg. This would suggest that oxidative phosphorylation is the sole process producing ATP until PO_2 levels fall to nearly zero.

The *in vivo* PQM technique used in this project demonstrates that the mitochondria appear to consume oxygen at rates that are dependent on PO_2 over a much wider physiological range. Since the rate of consumption varies based on oxygen tension, it may be the case that oxidative phosphorylation and glycolysis work simultaneously at a ratio that is dependent on PO_2. In situations where PO_2 is decreasing, for example, the cell would increasingly shift to using glycolysis to produce some of its ATP. Furthermore, when oxygen is abundant, the cell would shift to a higher utilization of oxidative phosphorylation. This PO_2-dependent ratio of oxidative phosphorylation and glycolysis differs from the classic view, but is more consistent with the oxygen dependence of respiration described in this project and previous similar studies (Golub, 2012).

The differences in values for half maximal respiration reported in earlier studies (Chance B., 1988) and those reported by Golub and Pittman are likely due to technical limitations. In the older studies, in-vitro techniques were used that involved suspensions of mitochondria or cells to measure oxygen consumption. A variety of error sources were likely introduced that led to vastly different results. Those potential sources of error were dramatically reduced when the in-vivo technique was implemented.

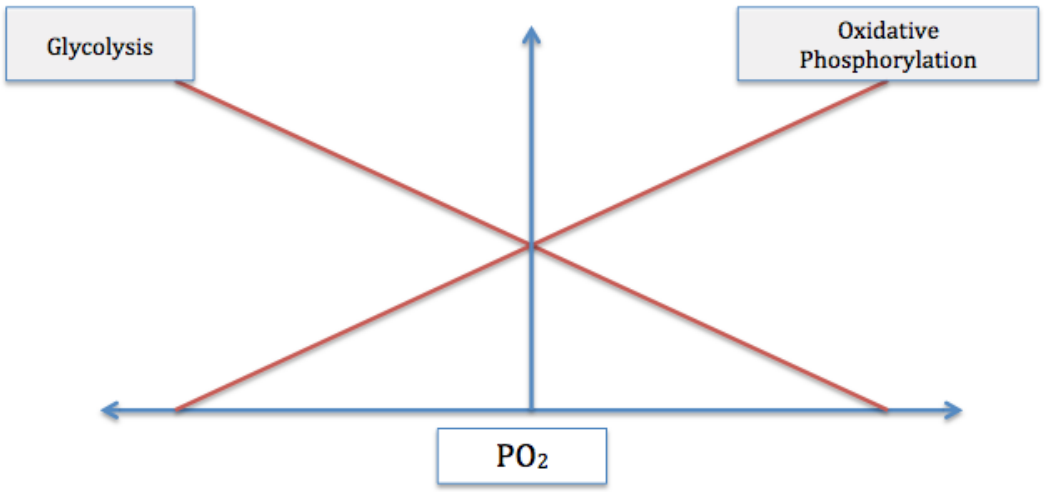

Figure 6. This is an illustration of the possible relationship between oxidative phosphorylation and glycolysis based on variations in PO_2. In this diagram, if PO_2 falls, the utilization of oxidative phosphorylation proportionally decreases as glycolysis increases.

Limitations and Future Studies

Although blood glucose concentrations were measured before and after each experiment, these animals were not fasted and it was not possible to determine how recently they had consumed rat chow. A more controlled eating schedule prior to experimentation may provide more consistent blood glucose levels. To monitor blood glucose, a single glucose reading was taken with the hand held glucometer. A more continuous system to monitor glucose may provide interesting correlations in oxygen consumption and glucose levels.

The rate of blood flow in the muscle was not measured in this project. Since blood flow is directly related to oxygen delivery to muscles, measuring this variable could improve the understanding of oxygen consumption measurements.

Additionally, the muscles studied were at rest. Inducing contraction while measuring PO_2 could help show how consumption rates are affected by an actively contracting muscle in healthy and diabetic rats.

It is relevant to note that a relatively small number of muscles were studied. More trials would be beneficial to more strongly validate the results obtained in this project and help clarify the observed differences in G-K and Wistar oxygen consumption characteristics.

The PQM technique used in this study utilized a 1 Hz flash rate, which provided a PO_2 reading every second. In future studies, the frequency of the laser flash rate could be increased to provide improved PO_2 resolution of the curves describing the PO_2 dependence of VO_2. This would, of course, require a different correction for the magnitude of photo-consumption by the method. More accurate Hill parameters may come from an increased flash frequency. Additionally, one could study oxygen consumption rate in diseased rats of different ages. The symptoms of the G-K rats used in this study progress over time much like the disease progresses in human diabetic patients. It would be interesting to compare an older, more "end-stage" diabetic rat with higher rates of microvascular complications to a younger rat. Since this method for studying the PO_2 dependence of oxygen consumption is relatively new, it would also be beneficial to determine if other chronic diseases such as hypertension or obesity would have an effect on consumption rates.

Conclusion

In conclusion, this project utilized a method of measuring the PO_2 of the interstitial fluid in spinotrapezius muscles of diabetic and non-diabetic rats. By arresting blood flow, the rate of oxygen disappearance due to respiration was calculated and differences between diseased and control rats were studied. The maximum rate of consumption for G-K rats was significantly higher than that of the Wistar control rats. The P_{50} for both rat sub-strains demonstrated oxygen consumption rates that depended on PO_2 over a wide physiological range. This elevated maximum rate of consumption in spontaneously diabetic rats should be investigated further to help better understand the effect of the disease on cellular respiration and on functional consequences of a mismatch between oxygen supply and demand.

References

Akash, M., Rehman, K., & Chen, S. (2013). Goto-kakizaki Rats: Its Suitability as Non-obese Diabetic Animal Model for Spontaneous Type 2 Diabetes Mellitus. *Current Diabetes Reviews,9*(5), 387-396. doi:10.2174/15733998113099990069

Belichenko, V. M., Baranov, V. I., Novosel'tsev, S. V., & Shoshenko, K. A. (2001). Coefficient of oxygen diffusion in fibers of the skeletal muscles. *Aviakosmicheskaia i ekologicheskaia meditsina= Aerospace and environmental medicine*, *36*(3), 31-38.

Bilz S. Sono S. Pypaert M. Shulman GI. Reduced mitochondrial density and increased IRS-1 serine phosphorylation in muscle of insulin-resistant offspring of type 2 diabetic parents. J Clin Invest. 2005;115:3587–3593.

Caroline Thomas, MB ChB FRCA, Andrew B Lumb, MB BS FRCA; Physiology of haemoglobin. Contin Educ Anaesth Crit Care Pain 2012; 12 (5): 251-256. doi: 10.1093/bjaceaccp/mks025

Chance B. Early reduction of cytochrome c in hypoxia. FEBS Lett 226: 343-346, 1988

Chance, B., & Williams, G. R. (1956). The respiratory chain and oxidative phosphorylation. *Adv Enzymol Relat Areas Mol Biol*, *17*, 65-134.

Chandel, N. S., & Schumacker, P. T. (2000). Cellular oxygen sensing by mitochondria: old questions, new insight. *Journal of applied physiology*, *88*(5), 1880-1889.

Constanzo, L.S. (1998). Physiology.Philadelphia, W.B. Saunders Company.

Gnaiger, E., Steinlechner-Maran, R., Méndez, G., Eberl, T., & Margreiter, R. (1995). Control of mitochondrial and cellular respiration by oxygen. *Journal of bioenergetics and biomembranes*, *27*(6), 583-596.

Golub, A. S., & Pittman, R. N. (2003). Thermostatic animal platform for intravital microscopy of thin tissues. *Microvascular research*, *66*(3), 213-217.

Golub, A. S., & Pittman, R. N. (2012). Oxygen dependence of respiration in rat spinotrapezius muscle in situ. *AJP: Heart and Circulatory Physiology,303*(1). doi:10.1152/ajpheart.00131.2012

Golub, A. S., Tevald, M. A., & Pittman, R. N. (2010). Phosphorescence quenching microrespirometry of skeletal muscle in situ. *AJP: Heart and Circulatory Physiology,300*(1). doi:10.1152/ajpheart.00626.2010

Goto, Y., Kakizaki, M., & Masaki, N. (1976). Production of Spontaneous Diabetic Rats by Repetition of Selective Breeding. *The Tohoku Journal of Experimental Medicine,119*(1), 85-90. doi:10.1620/tjem.119.85

Gray SD. Rat spinotrapezius muscle preparation for microscopic observation of the terminal vascular bed. Microvasc Res 5: 395-400, 1973.

Kelley DE. He J. Menshikova EV. Ritov VB. Dysfunction of mitochondria in human skeletal muscle in type 2 diabetes. Diabetes. 2002;51:2944–2950.

Meetoo, D; McGovern, P; Safadi, R (13–27 September 2007). "An epidemiological overview of diabetes across the world". British journal of nursing (Mark Allen Publishing). 16 (16): 1002–7. PMID 18026039

Mookerjee SA, Divakaruni AS, Jastroch M, Brand MD. Mitochondrial uncoupling and lifespan. *Mechanisms of ageing and development*. 2010;131(7-8):463-472. doi:10.1016/j.mad.2010.03.010.

Morino K. Petersen KF. Dufour S. Befroy D. Frattini J. Shatzkes N. Neschen S. White MF.

Nugent, W. H., Song, B. K., Pittman, R. N., & Golub, A. S. (2016). Simultaneous sampling of tissue oxygenation and oxygen consumption in skeletal muscle. *Microvascular Research,105*, 15-22. doi:10.1016/j.mvr.2015.12.007

Pishchany G, Skaar EP. Taste for Blood: Hemoglobin as a Nutrient Source for Pathogens. Heitman J, ed. *PLoS Pathogens*. 2012;8(3):e1002535. doi:10.1371/journal.ppat.1002535.

Pittman, R. N. (2011). *Regulation of tissue oxygenation*. San Rafael, CA: Morgan & Claypool.

Schenkman, K. A., Marble, D. R., Burns, D. H., & Feigl, E. O. (1997). Myoglobin oxygen dissociation by multiwavelength spectroscopy. *Journal of Applied Physiology*, *82*(1), 86-92.

Sivitz WI, Yorek MA. Mitochondrial Dysfunction in Diabetes: From Molecular Mechanisms to Functional Significance and Therapeutic Opportunities. *Antioxidants & Redox Signaling*. 2010;12(4):537-577. doi:10.1089/ars.2009.2531.

Sivitz, William I., and Mark A. Yorek. “Mitochondrial Dysfunction in Diabetes: From Molecular Mechanisms to Functional Significance and Therapeutic Opportunities.” Antioxidants & Redox Signaling 12.4 (2010): 537–577. PMC. Web. 19 Apr. 2017.

White, M. F. (1998). The IRS-signalling system: a network of docking proteins that mediate insulin action. In *Insulin Action* (pp. 3-11). Springer US.

Wilson DF, Erecinska M. Effect of oxygen concentration on cellular metabolism. Chest 88: 229S-232S, 1985.

Wilson DF, Oxygen pressures in the interstitial space and their relationship to those in the blood plasma in resting skeletal muscle. (2006) J Appl Physiol 101: 1648

Wilson, D. F., Harrison, D. K., & Vinogradov, S. A. (2012). Oxygen, pH, and mitochondrial oxidative phosphorylation. *Journal of Applied Physiology,113*(12), 1838-1845. doi:10.1152/japplphysiol.01160.2012

Wilson, D. F., Rumsey, W. L., Green, T. J., & Vanderkooi, J. (1988). The oxygen dependence of mitochondrial oxidative phosphorylation measured by a new optical method for measuring oxygen concentration. *Journal of Biological Chemistry*, *263*(6), 2712-2718.

Appendix

Wistar VO_2 vs. PO_2 plots

A – PO_2 (mmHg)

B- VO_2 (nl $O_2/(cm^3*s)$)

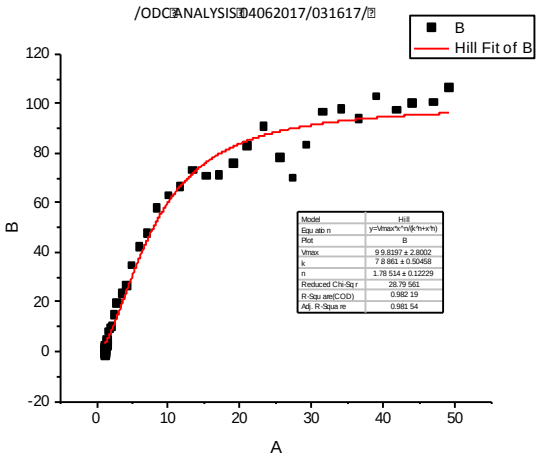

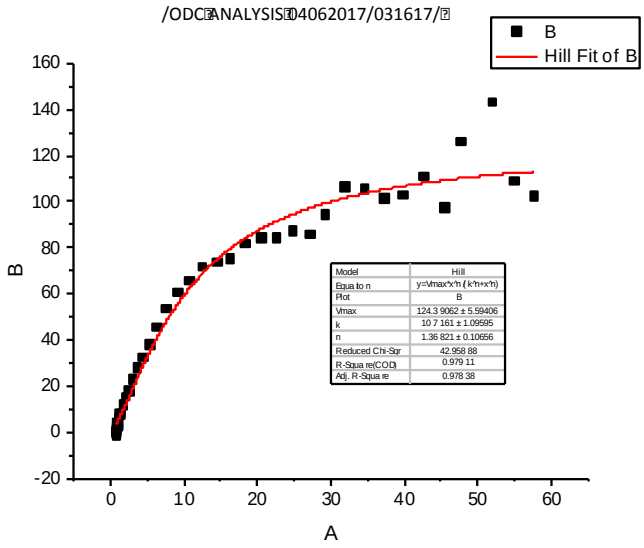

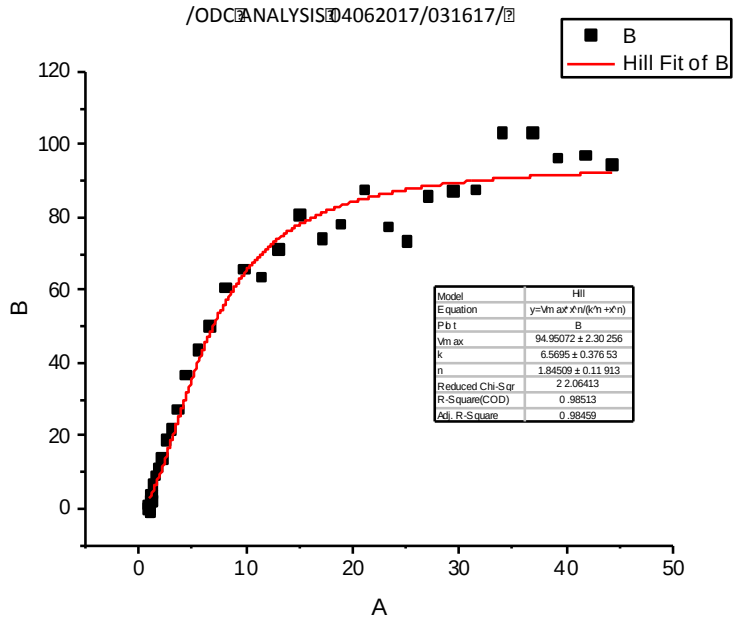
/ODC ANALYSIS 04062017/031617/
B
Hill Fit of B
B
A
Model Hill
Equation y=Vm ax*x^n/(k^n +x^n)
Plot B
Vm ax 94.95072 ± 2.30 256
k 6.5695 ± 0.376 53
n 1.84509 ± 0.11 913
Reduced Chi-Sqr 2 2.06413
R-Square(COD) 0 .98513
Adj. R-Square 0 .98459

3

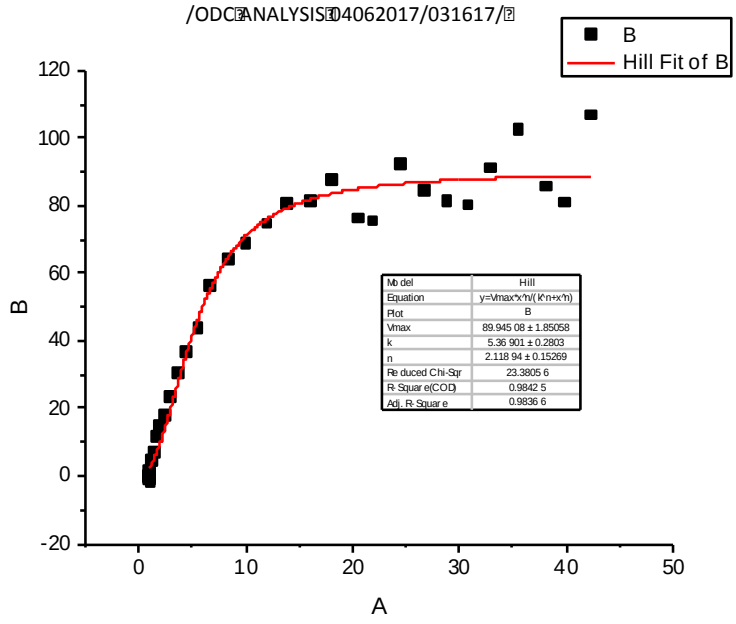
/ODC ANALYSIS 04062017/031617/
B
Hill Fit of B
B
A
Mo del Hill
Equation y=Vmax*x^n/(k^n+x^n)
Plot B
Vmax 89.945 08 ± 1.85058
k 5.36 901 ± 0.2803
n 2.118 94 ± 0.15269
Re duced Chi-Sqr 23.3805 6
R-Squar e(COD) 0.9842 5
Adj. R-Squar e 0.9836 6

4

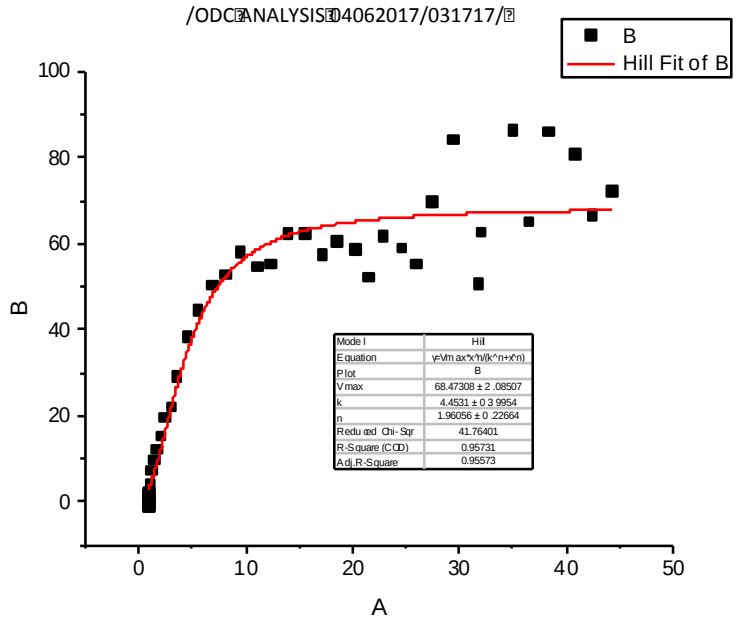
/ODC ANALYSIS 04062017/031717/
B
Hill Fit of B
B
A
Model | Hill
Equation | y=Vmax*x^n/(k^n+x^n)
Plot | B
Vmax | 68.47308 ± 2.08507
k | 4.4531 ± 0.39954
n | 1.96056 ± 0.22664
Reduced Chi-Sqr | 41.76401
R-Square (COD) | 0.95731
Adj. R-Square | 0.95573

5

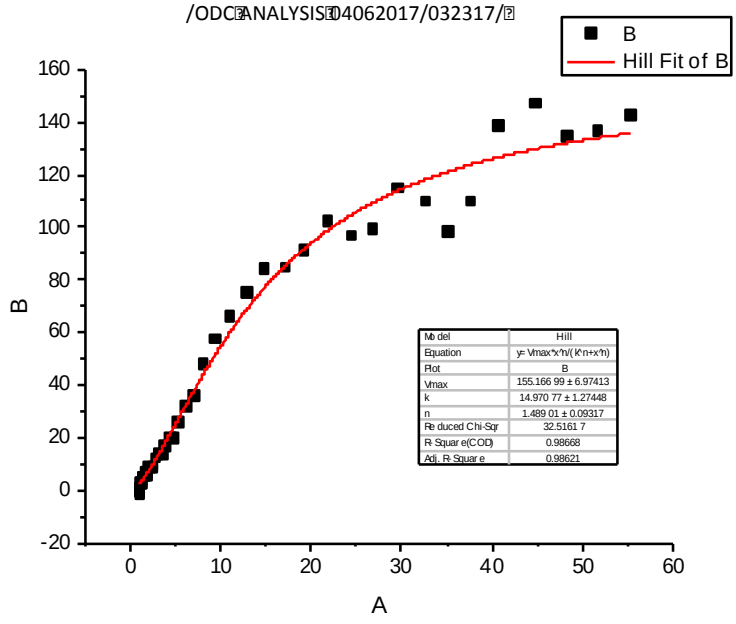
/ODC ANALYSIS 04062017/032317/
B
Hill Fit of B
B
A
Model | Hill
Equation | y= Vmax*x^n/(k^n+x^n)
Plot | B
Vmax | 155.16699 ± 6.97413
k | 14.97077 ± 1.27448
n | 1.48901 ± 0.09317
Reduced Chi-Sqr | 32.51617
R-Square(COD) | 0.98668
Adj. R-Square | 0.98621

6

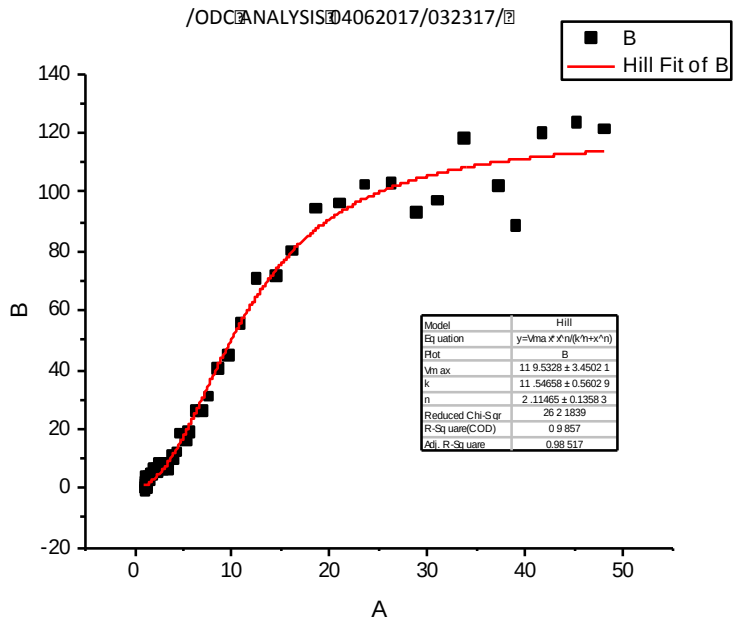
/ODC ANALYSIS 04062017/032317/
B
Hill Fit of B
B
A
Model Hill
Equation y=Vmax*x^n/(k^n+x^n)
Plot B
Vmax 11 9.5328 ± 3.4502 1
k 11 .54658 ± 0.5602 9
n 2 .11465 ± 0.1358 3
Reduced Chi-Sqr 26 2 1839
R-Square(COD) 0 9 857
Adj. R-Square 0.98 517

7

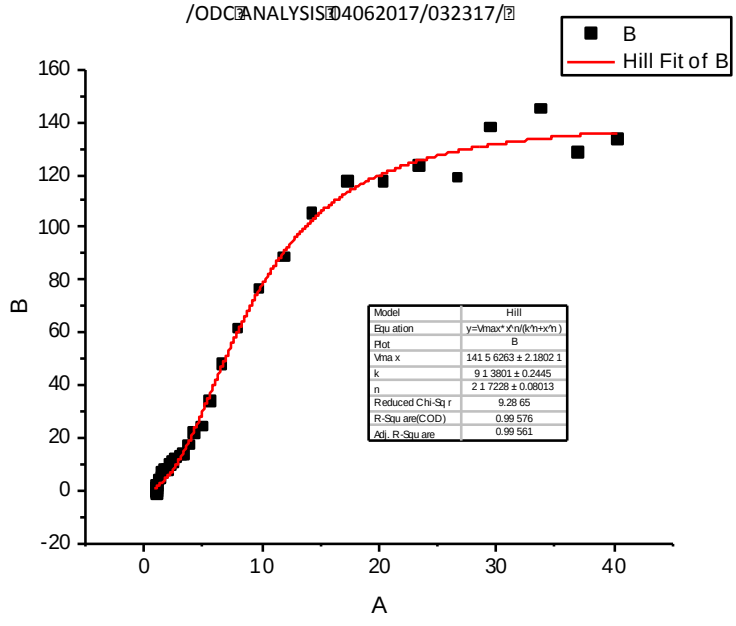
/ODC ANALYSIS 04062017/032317/
B
Hill Fit of B
B
A
Model Hill
Equation y=Vmax*x^n/(k^n+x^n)
Plot B
Vmax 141 5 6263 ± 2.1802 1
k 9 1 3801 ± 0.2445
n 2 1 7228 ± 0.08013
Reduced Chi-Sqr 9.28 65
R-Square(COD) 0.99 576
Adj. R-Square 0.99 561

8

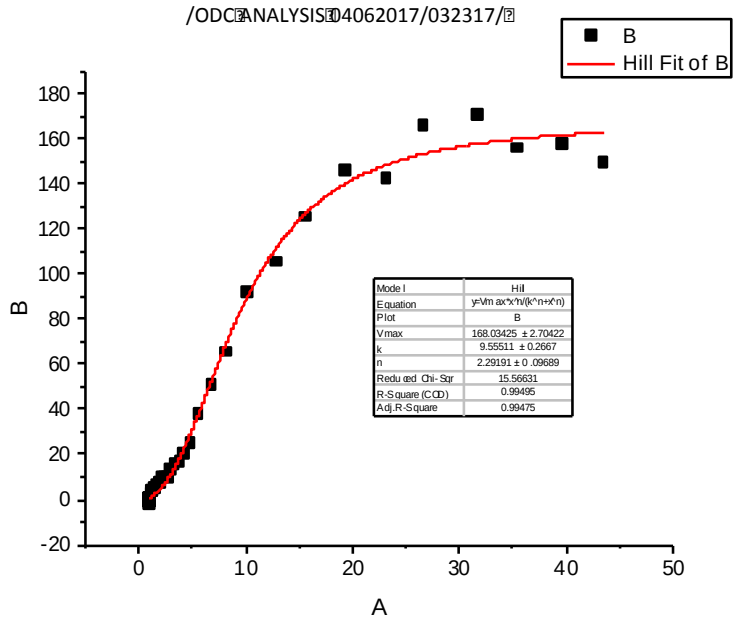
/ODC ANALYSIS 04062017/032317/
B
Hill Fit of B
B
A
Model Hill
Equation y=Vmax*x^n/(k^n+x^n)
Plot B
Vmax 168.03425 ± 2.70422
k 9.55511 ± 0.2667
n 2.29191 ± 0 .09689
Reduced Chi-Sqr 15.56631
R-Square (COD) 0.99495
Adj.R-Square 0.99475

9

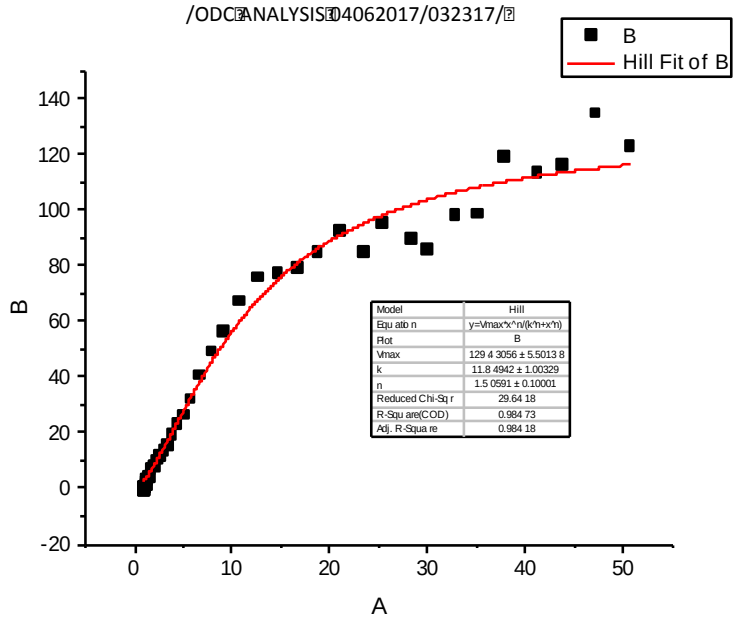
/ODC ANALYSIS 04062017/032317/
B
Hill Fit of B
B
A
Model Hill
Equation y=Vmax*x^n/(k^n+x^n)
Plot B
Vmax 129 4 3056 ± 5.5013 8
k 11.8 4942 ± 1.00329
n 1.5 0591 ± 0.10001
Reduced Chi-Sqr 29.64 18
R-Square(COD) 0.984 73
Adj. R-Squa re 0.984 18

10

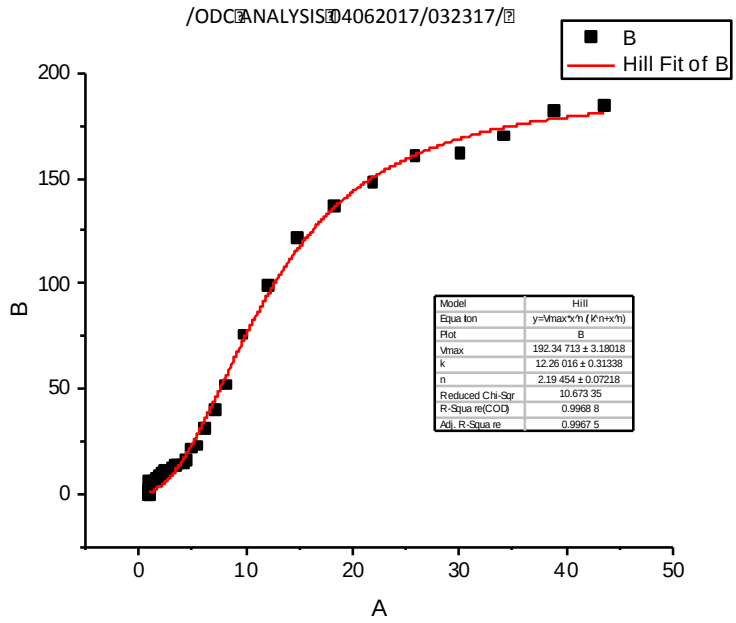
/ODC ANALYSIS 04062017/032317/
B
Hill Fit of B
Model Hill
Equation y=Vmax*x^n / (k^n+x^n)
Plot B
Vmax 192.34713 ± 3.18018
k 12.26016 ± 0.31338
n 2.19454 ± 0.07218
Reduced Chi-Sqr 10.67335
R-Square(COD) 0.99688
Adj. R-Square 0.99675
B
A
200
150
100
50
0
0
10
20
30
40
50

11

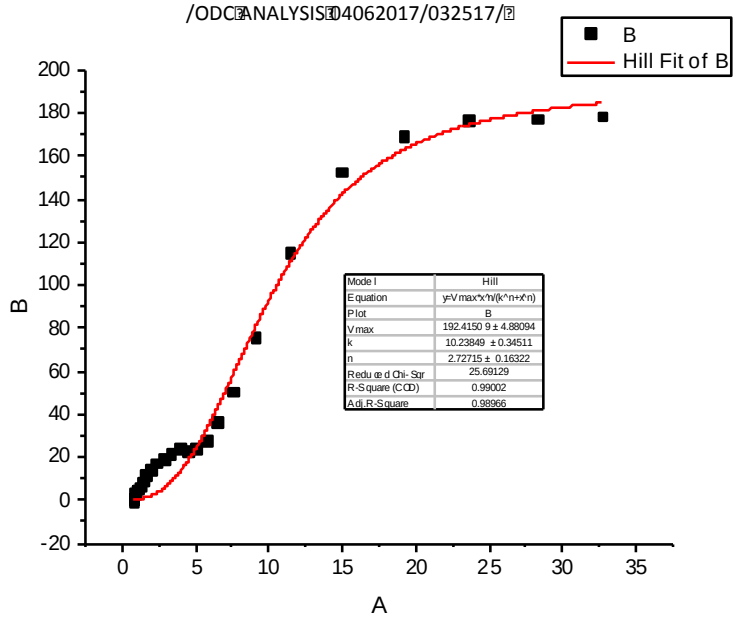
/ODC ANALYSIS 04062017/032517/
B
Hill Fit of B
Model Hill
Equation y=V max*x^n/(k^n+x^n)
Plot B
Vmax 192.41509 ± 4.88094
k 10.23849 ± 0.34511
n 2.72715 ± 0.16322
Reduced Chi-Sqr 25.69129
R-Square (COD) 0.99002
Adj. R-Square 0.98966
B
A
200
180
160
140
120
100
80
60
40
20
0
-20
0
5
10
15
20
25
30
35

12

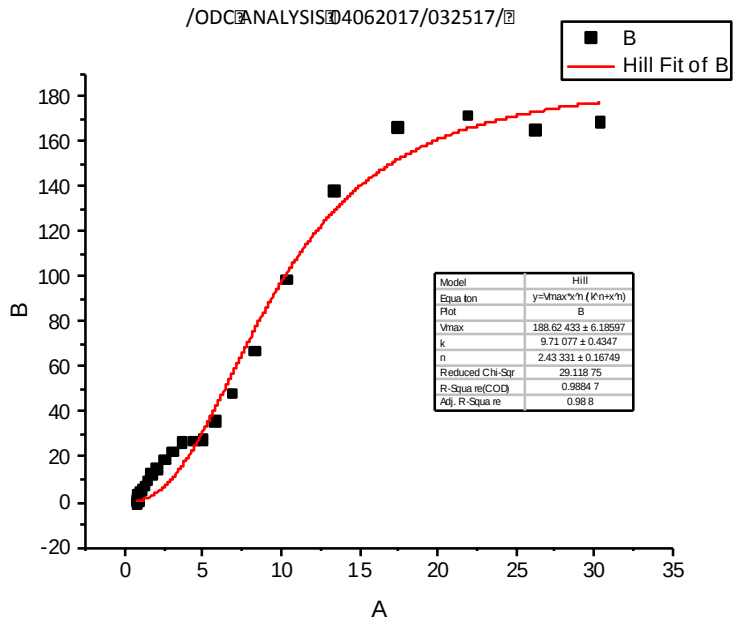
/ODC ANALYSIS 04062017/032517/
B
Hill Fit of B
B
A
Model Hill
Equation y=Vmax*x^n / (k^n+x^n)
Plot B
Vmax 188.62 433 ± 6.18597
k 9.71 077 ± 0.4347
n 2.43 331 ± 0.16749
Reduced Chi-Sqr 29.118 75
R-Squa re(COD) 0.9884 7
Adj. R-Squa re 0.98 8

13

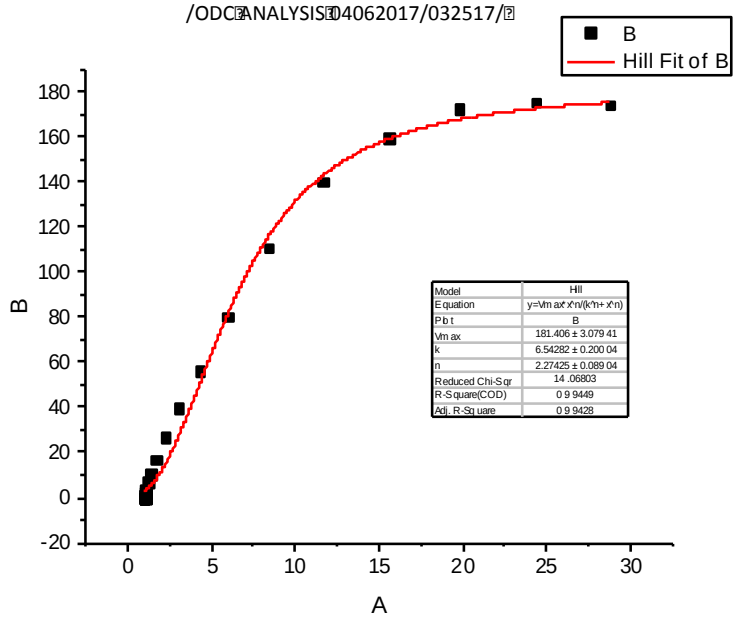
/ODC ANALYSIS 04062017/032517/
B
Hill Fit of B
B
A
Model Hill
Equation y=Vm ax* x^n/(k^n+ x^n)
Plo t B
Vm ax 181.406 ± 3.079 41
k 6.54282 ± 0.200 04
n 2.27425 ± 0.089 04
Reduced Chi-S qr 14 .06803
R-Square(COD) 0 9 9449
Adj. R-Sq uare 0 9 9428

14

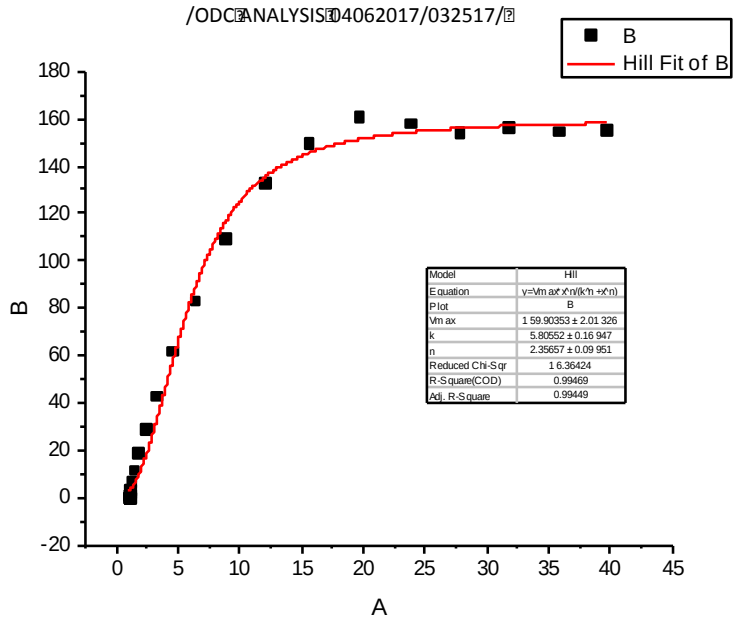
/ODC ANALYSIS 04062017/032517/
B
Hill Fit of B
B
A
Model Hill
Equation y=Vmax*x^n/(k^n +x^n)
Plot B
Vmax 1 59.90353 ± 2.01 326
k 5.80552 ± 0.16 947
n 2.35657 ± 0.09 951
Reduced Chi-Sqr 1 6.36424
R-Square(COD) 0.99469
Adj. R-Square 0.99449

15

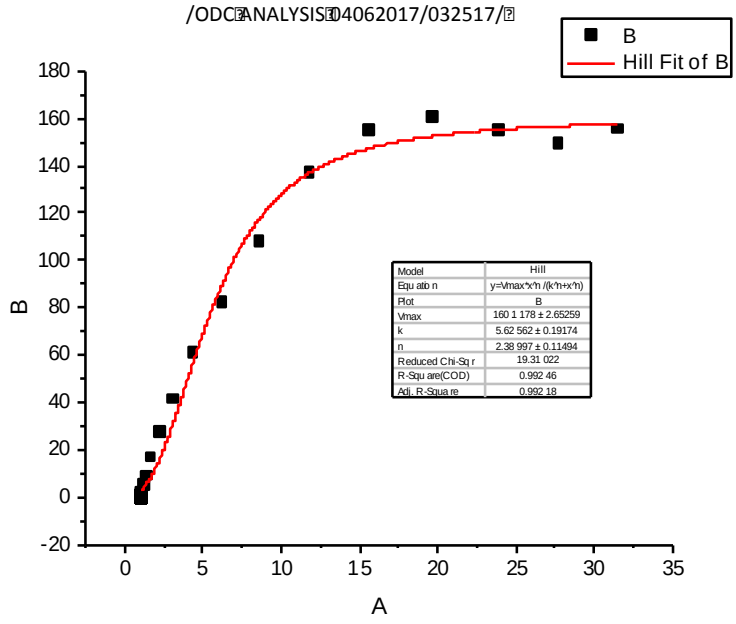
/ODC ANALYSIS 04062017/032517/
B
Hill Fit of B
B
A
Model Hill
Equ atio n y=Vmax*x^n /(k^n+x^n)
Plot B
Vmax 160 1 178 ± 2.65259
k 5.62 562 ± 0.19174
n 2.38 997 ± 0.11494
Reduced Chi-Sq r 19.31 022
R-Squ are(COD) 0.992 46
Adj. R-Squa re 0.992 18

16

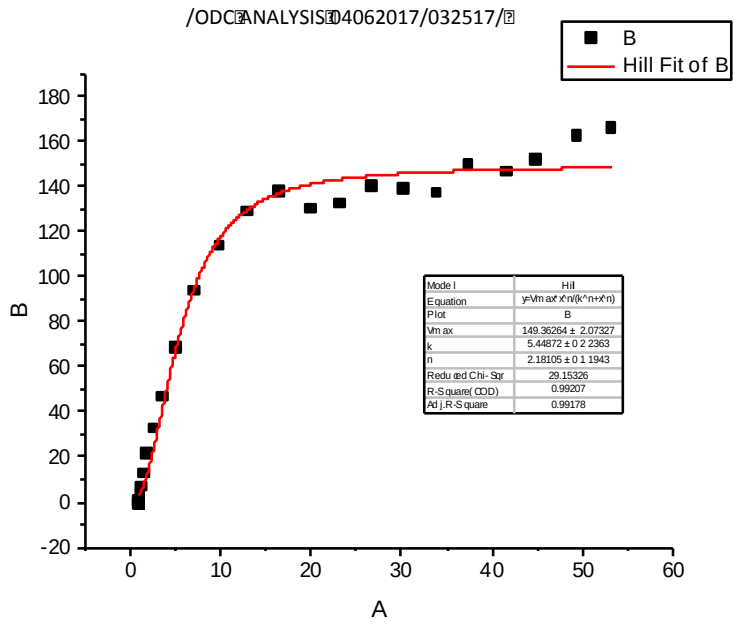
/ODC ANALYSIS 04062017/032517/
B
Hill Fit of B
B
A
Model Hill
Equation y=Vmax*x^n/(k^n+x^n)
Plot B
Vmax 149.36264 ± 2.07327
k 5.44872 ± 0.22363
n 2.18105 ± 0.11943
Reduced Chi-Sqr 29.15326
R-Square(COD) 0.99207
Adj. R-Square 0.99178

17

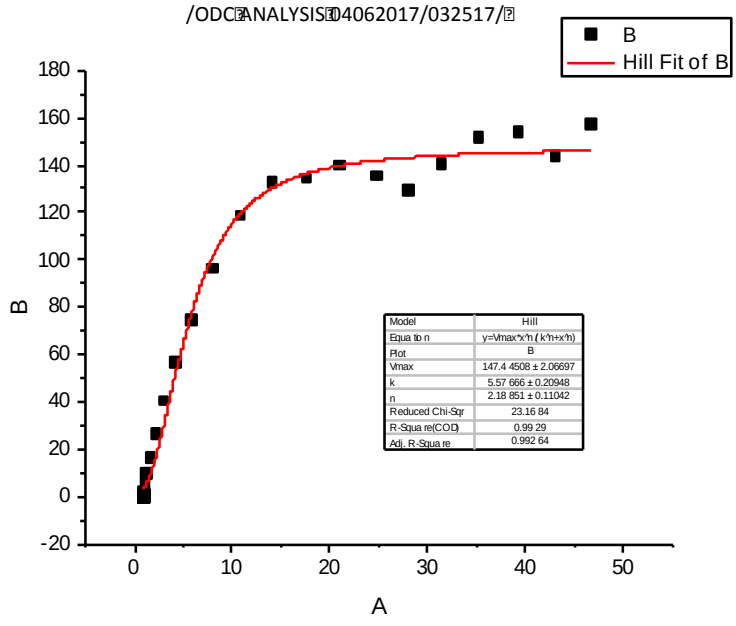
/ODC ANALYSIS 04062017/032517/
B
Hill Fit of B
B
A
Model Hill
Equation y=Vmax*x^n/(k^n+x^n)
Plot B
Vmax 147.44508 ± 2.06697
k 5.57666 ± 0.20948
n 2.18851 ± 0.11042
Reduced Chi-Sqr 23.1684
R-Square(COD) 0.9929
Adj. R-Square 0.99264

18

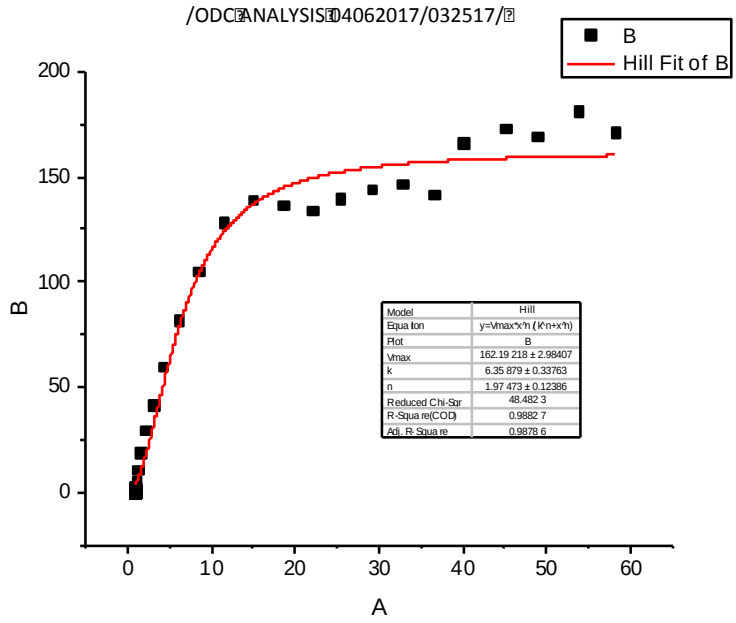
/ODC ANALYSIS 04062017/032517/
B
Hill Fit of B
200
150
100
50
0
B
0
10
20
30
40
50
60
A
Model Hill
Equation y=Vmax*x^n / (k^n+x^n)
Plot B
Vmax 162.19 218 ± 2.98407
k 6.35 879 ± 0.33763
n 1.97 473 ± 0.12386
Reduced Chi-Sqr 48.482 3
R-Square(COD) 0.9882 7
Adj. R-Square 0.9878 6

19

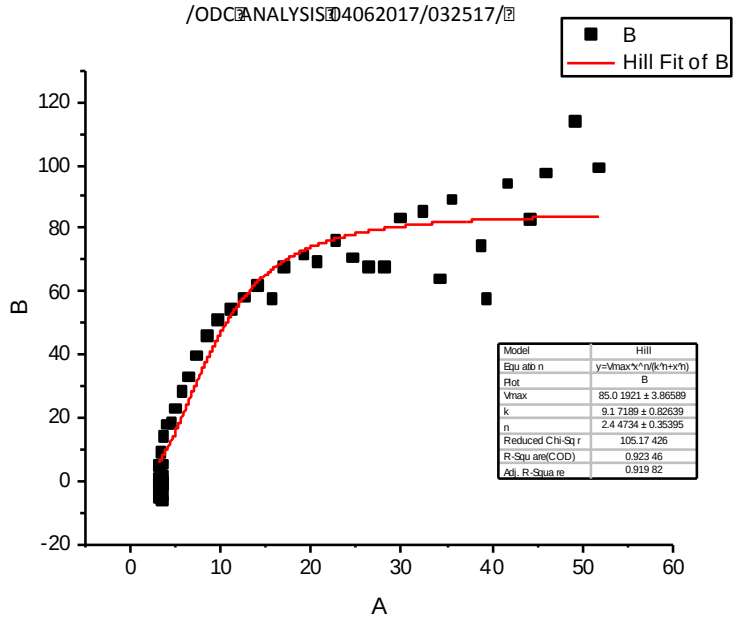
/ODC ANALYSIS 04062017/032517/
B
Hill Fit of B
120
100
80
60
40
20
0
-20
B
0
10
20
30
40
50
60
A
Model Hill
Equation y=Vmax*x^n/(k^n+x^n)
Plot B
Vmax 85.0 1921 ± 3.86589
k 9.1 7189 ± 0.82639
n 2.4 4734 ± 0.35395
Reduced Chi-Sqr 105.17 426
R-Square(COD) 0.923 46
Adj. R-Square 0.919 82

20

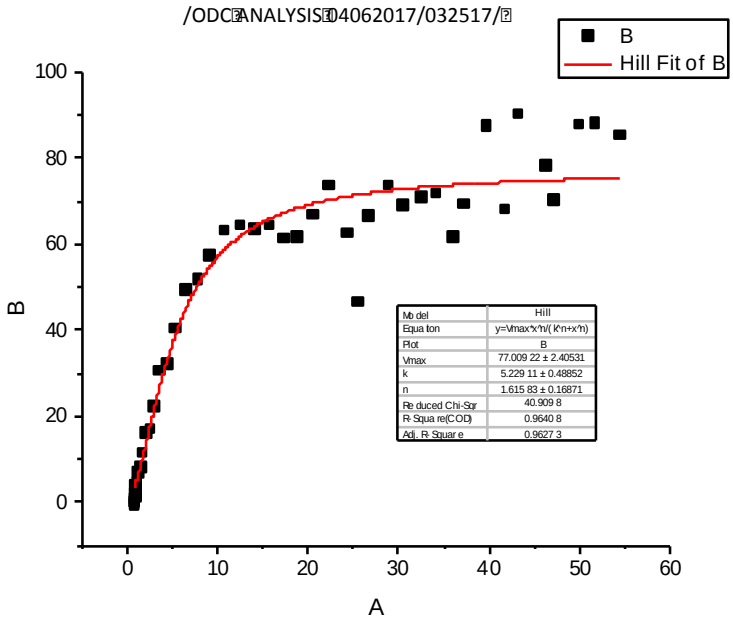
/ODC ANALYSIS 04062017/032517/
B
Hill Fit of B
100
80
60
40
20
0
B
0
10
20
30
40
50
60
A
Mo del
Hill
Equa tion
y=Vmax*x^n/(k^n+x^n)
Plot
B
Vmax
77.009 22 ± 2.40531
k
5.229 11 ± 0.48852
n
1.615 83 ± 0.16871
Re duced Chi-Squ
40.909 8
R-Squa re(COD)
0.9640 8
Adj. R-Squar e
0.9627 3

21

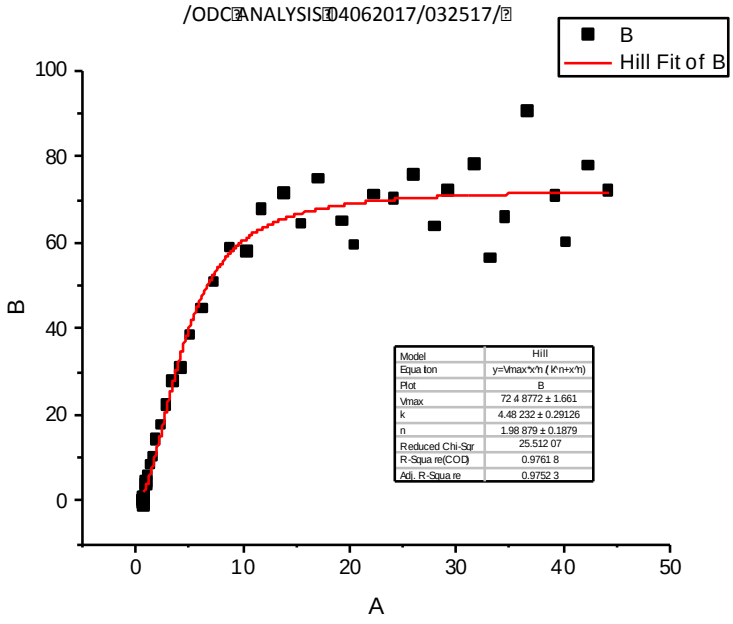
/ODC ANALYSIS 04062017/032517/
B
Hill Fit of B
100
80
60
40
20
0
B
0
10
20
30
40
50
A
Model
Hill
Equa tion
y=Vmax*x^n / (k^n+x^n)
Plot
B
Vmax
72 4 8772 ± 1.661
k
4.48 232 ± 0.29126
n
1.98 879 ± 0.1879
Reduced Chi-Squ
25.512 07
R-Squa re(COD)
0.9761 8
Adj. R-Squa re
0.9752 3

22

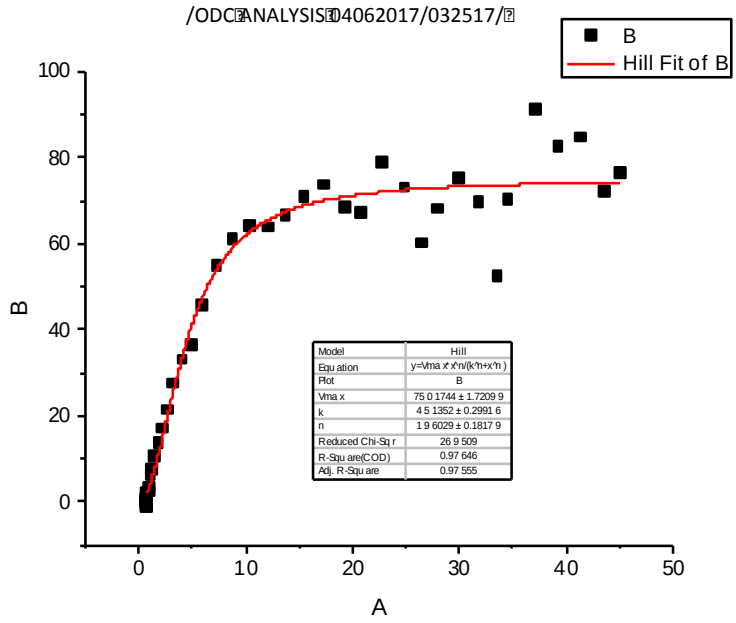
/ODC ANALYSIS 04062017/032517/
B
Hill Fit of B
100
80
60
40
20
0
B
0
10
20
30
40
50
A
Model Hill
Equation y=Vmax*x^n/(k^n+x^n)
Plot B
Vmax 75 0 1744 ± 1.7209 9
k 4 5 1352 ± 0.2991 6
n 1 9 6029 ± 0.1817 9
Reduced Chi-Sqr 26 9 509
R-Square(COD) 0.97 646
Adj. R-Square 0.97 555

23

Goto-Kakizaki VO_2 vs. PO_2 plots

A – PO_2 (mmHg)

B- VO_2 (nl $O_2/(cm^3*s)$)

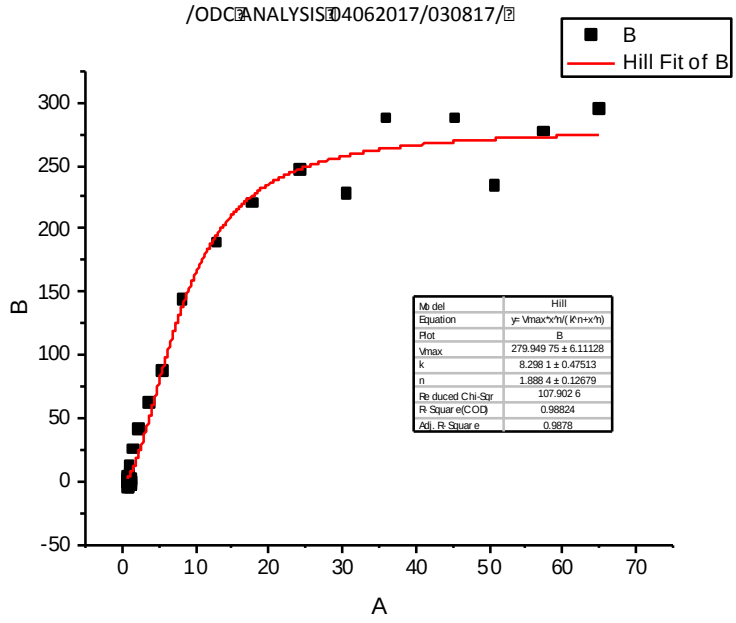

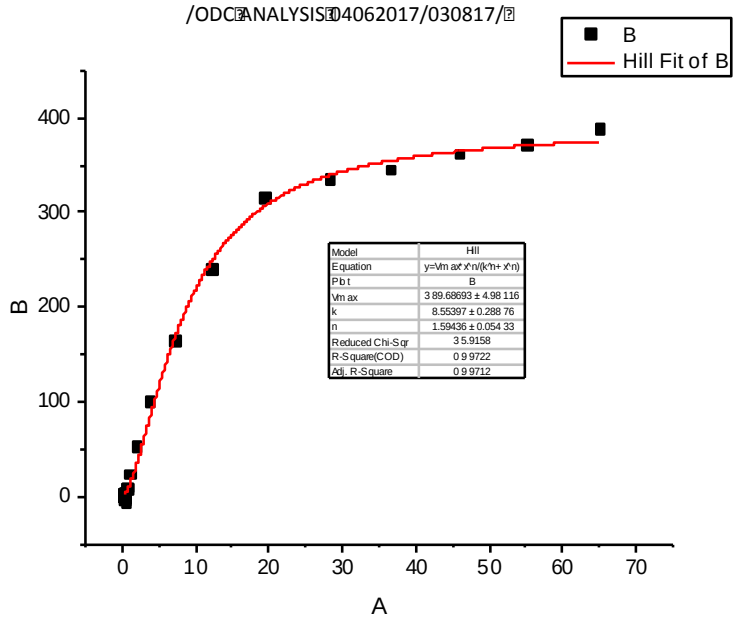

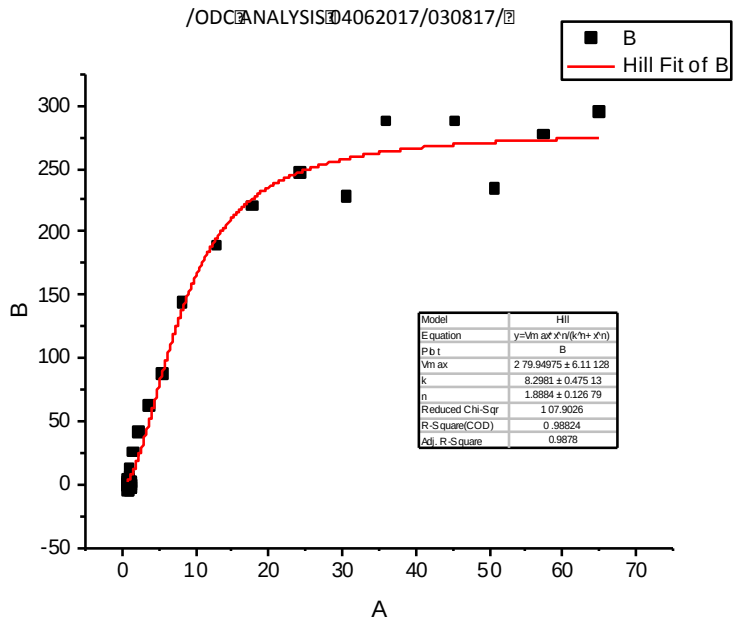
/ODC ANALYSIS 04062017/030817/
B
Hill Fit of B
B
A
Model Hill
Equation y=Vm ax*x^n/(k^n+ x^n)
Plot B
Vm ax 279.94975 ± 6.11128
k 8.2981 ± 0.47513
n 1.8884 ± 0.12679
Reduced Chi-Sqr 107.9026
R-Square(COD) 0.98824
Adj. R-Square 0.9878

3

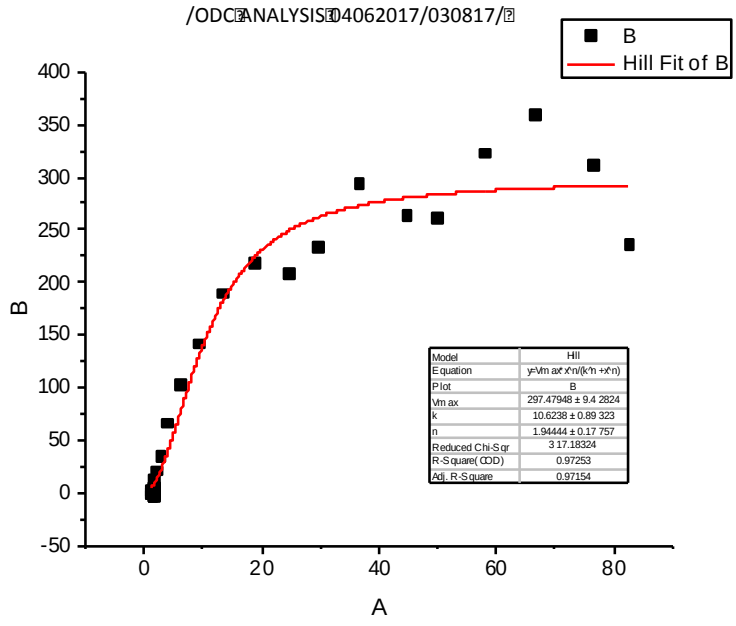
/ODC ANALYSIS 04062017/030817/
B
Hill Fit of B
B
A
Model Hill
Equation y=Vm ax*x^n/(k^n +x^n)
Plot B
Vm ax 297.47948 ± 9.42824
k 10.6238 ± 0.89323
n 1.94444 ± 0.17757
Reduced Chi-Sqr 317.18324
R-Square(COD) 0.97253
Adj. R-Square 0.97154

4

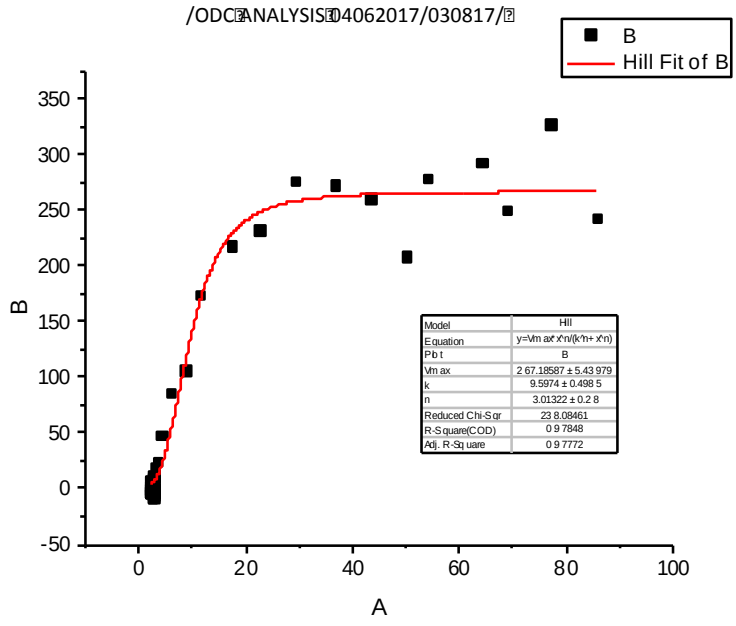
/ODC ANALYSIS 04062017/030817/
B
Hill Fit of B
B
A
Model Hill
Equation y=Vm ax*x^n/(k^n+ x^n)
Pb t B
Vm ax 2 67.18587 ± 5.43 979
k 9.5974 ± 0.498 5
n 3.01322 ± 0.2 8
Reduced Chi-Sqr 23 8.08461
R-Square(COD) 0 9 7848
Adj. R-Sq uare 0 9 7772

5

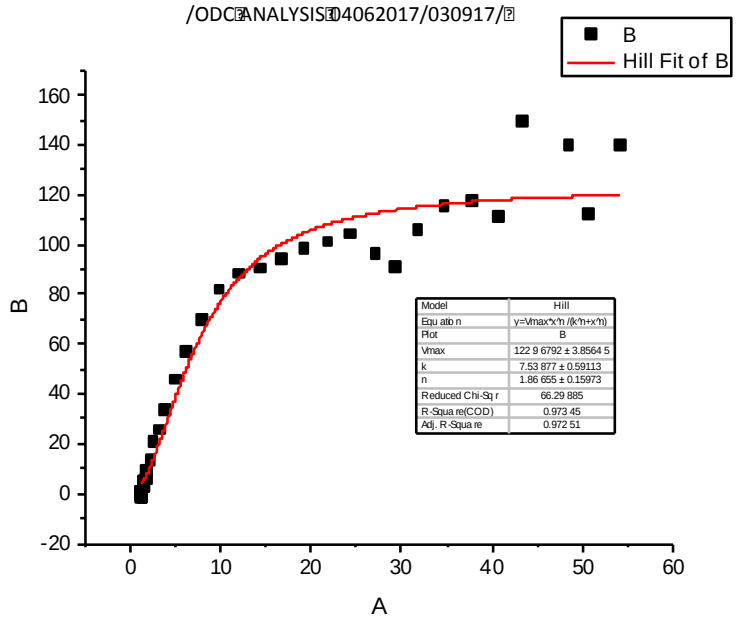
/ODC ANALYSIS 04062017/030917/
B
Hill Fit of B
B
A
Model Hill
Equ atio n y=Vmax*x^n /(k^n+x^n)
Plot B
Vmax 122 9 6792 ± 3.8564 5
k 7.53 877 ± 0.59113
n 1.86 655 ± 0.15973
Reduced Chi-Sq r 66.29 885
R-Squa re(COD) 0.973 45
Adj. R-Squa re 0.972 51

6

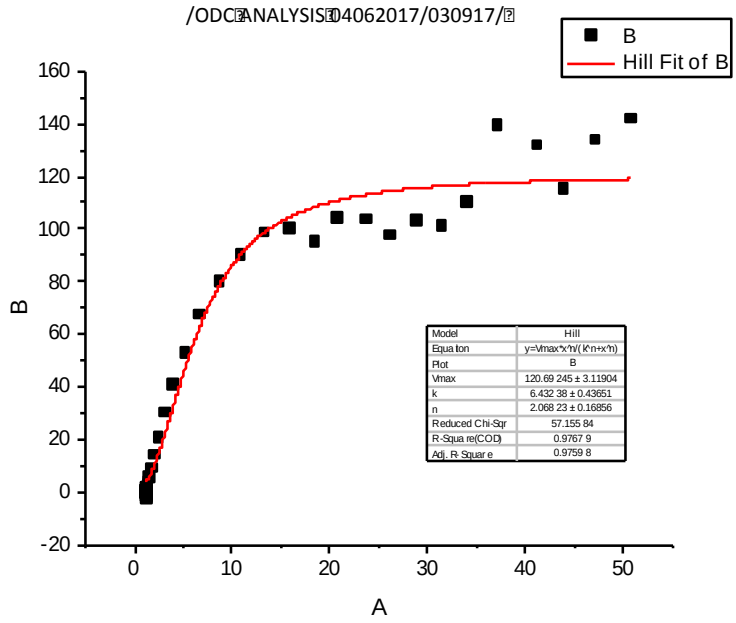
/ODC ANALYSIS 04062017/030917/
B
Hill Fit of B
160
140
120
100
80
60
40
20
0
-20
0
10
20
30
40
50
B
A
Model Hill
Equation y=Vmax*x^n/(k^n+x^n)
Plot B
Vmax 120.69245 ± 3.11904
k 6.43238 ± 0.43651
n 2.06823 ± 0.16856
Reduced Chi-Sqr 57.15584
R-Square(COD) 0.97679
Adj. R-Square 0.97598

7

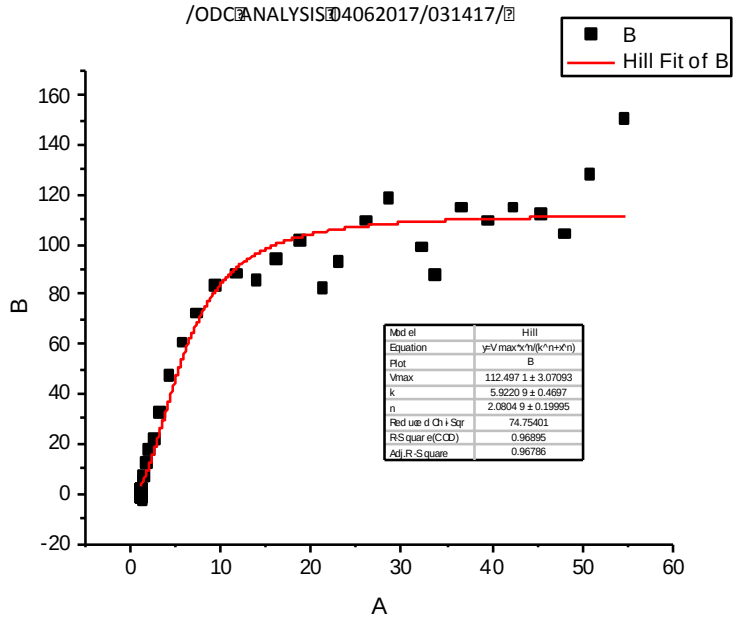
/ODC ANALYSIS 04062017/031417/
B
Hill Fit of B
160
140
120
100
80
60
40
20
0
-20
0
10
20
30
40
50
60
B
A
Model Hill
Equation y=Vmax*x^n/(k^n+x^n)
Plot B
Vmax 112.49771 ± 3.07093
k 5.92209 ± 0.4697
n 2.08049 ± 0.19995
Reduced Chi-Sqr 74.75401
R-Square(COD) 0.96895
Adj. R-Square 0.96786

8

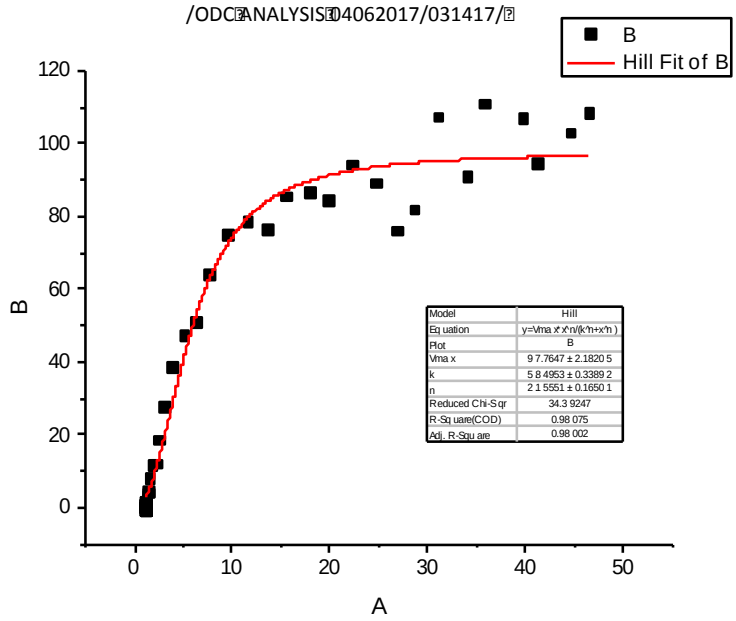
/ODC ANALYSIS 04062017/031417/
B
Hill Fit of B
B
A
Model Hill
Equation y=Vmax*x^n/(k^n+x^n)
Plot B
Vmax 97.7647 ± 2.18205
k 58.4953 ± 0.33892
n 2.15551 ± 0.16501
Reduced Chi-Sqr 34.39247
R-Square(COD) 0.98075
Adj. R-Square 0.98002

9

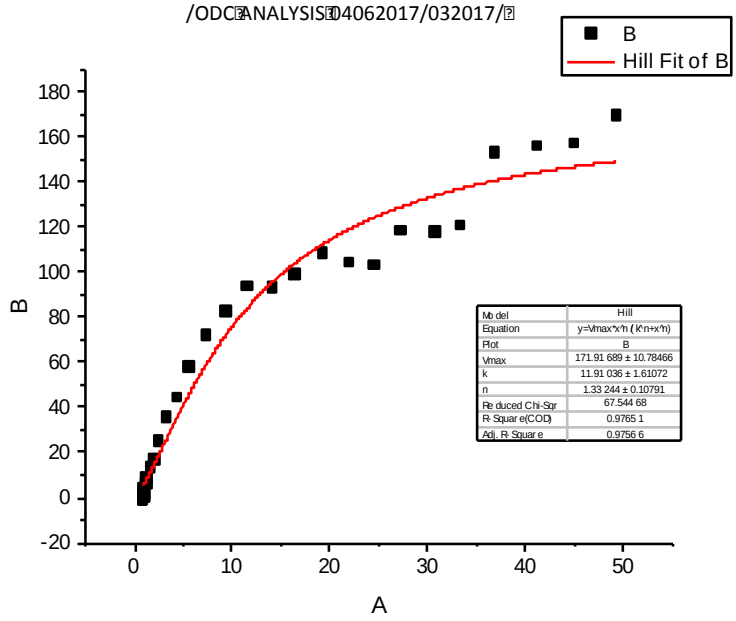
/ODC ANALYSIS 04062017/032017/
B
Hill Fit of B
B
A
Model Hill
Equation y=Vmax*x^n/(k^n+x^n)
Plot B
Vmax 171.91689 ± 10.78466
k 11.91036 ± 1.61072
n 1.33244 ± 0.10791
Reduced Chi-Sqr 67.54468
R-Square(COD) 0.97651
Adj. R-Square 0.97566

10

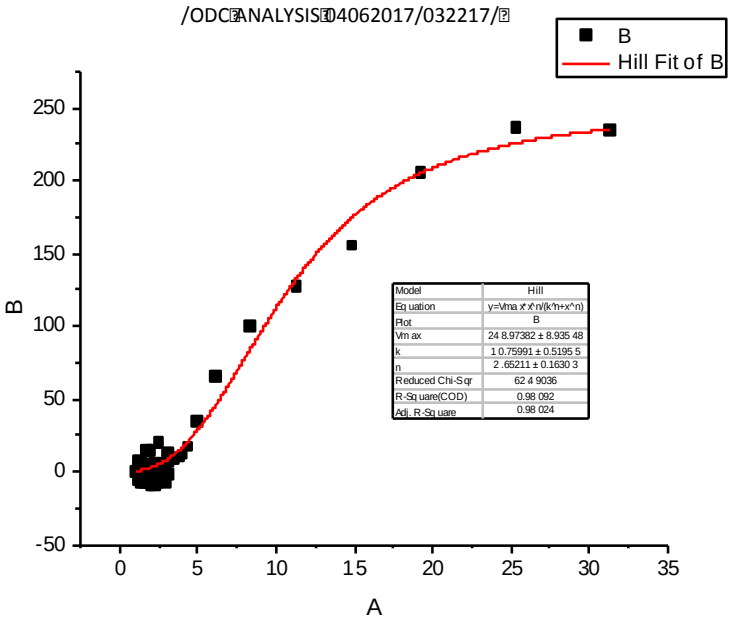
/ODC ANALYSIS 04062017/032217/
B
Hill Fit of B
250
200
150
100
50
0
-50
0
5
10
15
20
25
30
35
B
A
Model Hill
Equation y=Vma x*x^n/(k^n+x^n)
Plot B
Vmax 24 8.97382 ± 8.935 48
k 1 0.75991 ± 0.5195 5
n 2 .65211 ± 0.1630 3
Reduced Chi-Sqr 62 4 9036
R-Square(COD) 0.98 092
Adj. R-Square 0.98 024

11

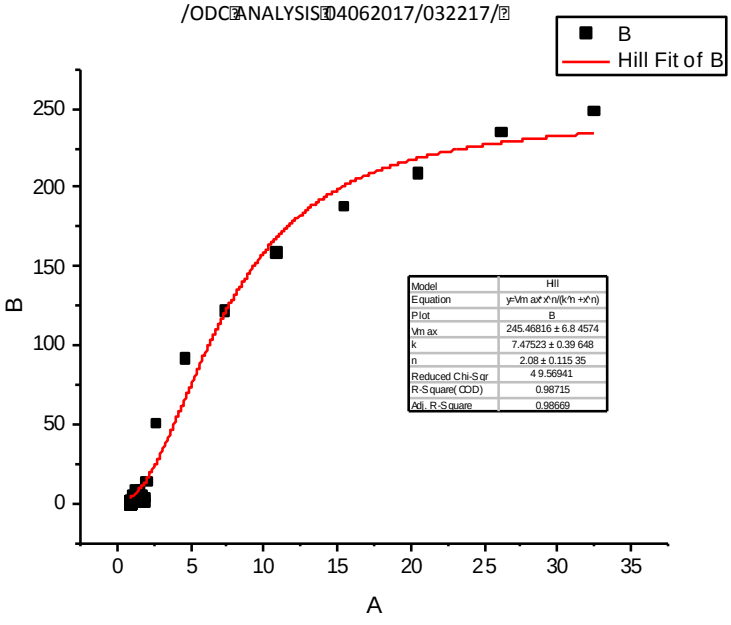
/ODC ANALYSIS 04062017/032217/
B
Hill Fit of B
250
200
150
100
50
0
0
5
10
15
20
25
30
35
B
A
Model Hill
Equation y=Vm ax*x^n/(k^n +x^n)
Plot B
Vmax 245.46816 ± 6.8 4574
k 7.47523 ± 0.39 648
n 2.08 ± 0.115 35
Reduced Chi-Sqr 4 9.56941
R-Square(COD) 0.98715
Adj. R-Square 0.98669

12

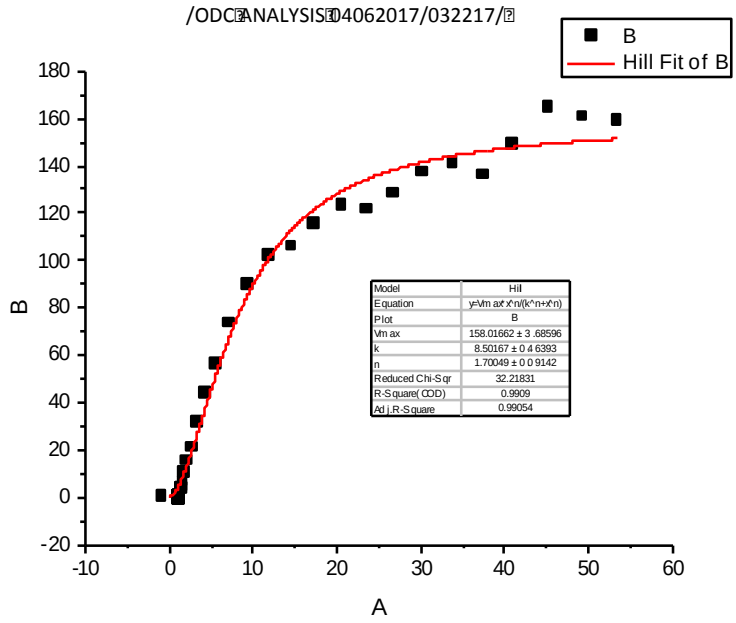
/ODC ANALYSIS 04062017/032217/
B
Hill Fit of B
B
A
Model Hill
Equation y=Vm ax*x^n/(k^n+x^n)
Plot B
Vm ax 158.01662 ± 3 .68596
k 8.50167 ± 0 4 6393
n 1.70049 ± 0 0 9142
Reduced Chi-Sqr 32.21831
R-Square(COD) 0.9909
Ad j.R-Square 0.99054

13

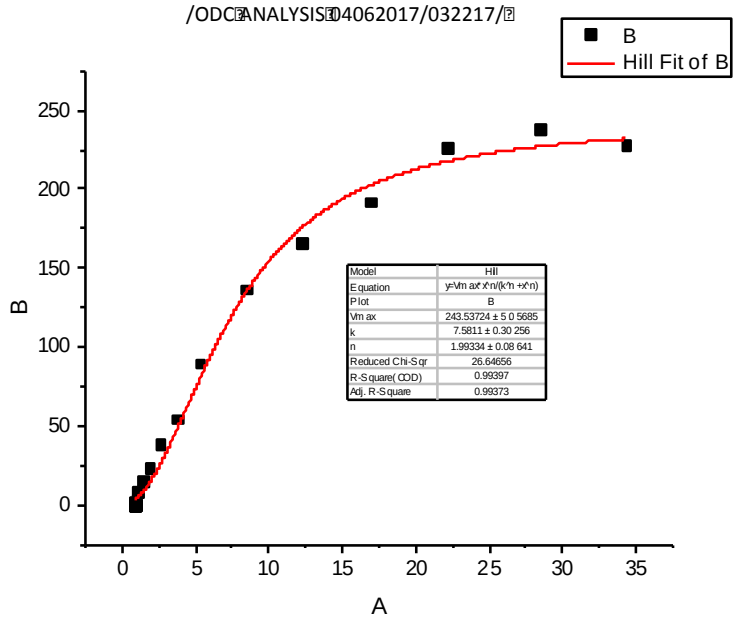
/ODC ANALYSIS 04062017/032217/
B
Hill Fit of B
B
A
Model Hill
Equation y=Vm ax*x^n/(k^n +x^n)
Plot B
Vm ax 243.53724 ± 5 0 5685
k 7.5811 ± 0.30 256
n 1.99334 ± 0.08 641
Reduced Chi-Sqr 26.64656
R-Square(COD) 0.99397
Adj. R-Square 0.99373

14

Vita

Alexander Cameron Liles was born on June 18, 1991 in Newport News, Virginia. He graduated from Menchville High School in June, 2009. He received his Bachelor of Science from Virginia Polytechnic Institute and State University in May, 2013 and went on to receive a Master of Science in Physiology and Biophysics from Virginia Commonwealth University in May, 2017.